SULFUR DEGASSING FROM MT. EREBUS VOLCANO, ANTARCTICA

Dawn Catherine Sweeney

Independent Study Submitted in Partial Fulfillment of the
requirements for the Degree of Masters of Science in
Geochemistry

New Mexico Institute of Mining and Technology

Socorro, New Mexico
September 2006

TABLE OF CONTENTS

LIST OF FIGURES

LIST OF TABLES

ABSTRACT

SO_2 emission rates from Erebus volcano show periodicity, which directly relates to lava lake convection and magma and conduit processes. Mt. Erebus is a 3794 m stratovolcano with a persistently degassing convecting, phonolite lava lake. Lava lake SO_2 emission rates were collected from 1992 to 2003 using the correlation spectrometer (COSPEC) and in 2003 and 2005 using a miniature ultra-violet differential optical absorption spectrometer (DOAS). COSPEC results show increasing emission rates from 39±17 Mg/day (0.5 kg/s) in 1996 to ~80±25 Mg/day (0.9 kg/s) in 2003. DOAS emission rates from 2003 and 2005 are nearly identical at ~80±26 Mg/day (0.9 kg/s). DOAS fluxes are within 10% of COSPEC fluxes when parameters like number of averaged spectra (coadds) and integration times of measured spectra are carefully selected to optimize data collection. At Erebus volcano, COSPEC performs more consistently than DOAS because of the high signal to noise ratio in the DOAS data. Time series analysis of SO_2 emission rates show periodicities that range from 10 minutes to 3 hours. Short cycles may be related to puffing at the lava lake surface and long cycles may be related to deeper conduit processes. Modeling suggests that Poiseuille flow is the most plausible model to explain magma convection in the conduit and lava lake. The contribution of volcanic S to the Antarctic atmospheric S budget increased from 1993 to 2006 from 3% to 4% whereas the contribution to the global atmospheric S budget increased from 0.03% to 0.04%.

ACKNOWLEDGEMENTS

Thanks to my advisor, Phil Kyle, for the opportunity to work on Erebus volcano and the knowledge gained while I was his student. Also, thanks to Clive Oppenheimer for teaching me the intricacies of DOAS. I am greatly indebted to my fellow student cohorts in this research project for their candidness and friendship during this entire process. They are Shauna Mikelich and Peter Kelly. Thanks to Lisa Peters and Rich Esser of New Mexico Geochronology Research Lab for discussions of various parts of my research. Thanks to Dr. Brian Borchers for helping with the time-series analysis work. Thanks to Jeff Sutton and Tamar Elias of Hawaiian Volcanoes Observatory for helping me understand volcanic monitoring better. Thanks to Bill McIntosh and Nelia Dunbar for help with writing, the microprobe and endless yoga discussions. Finally, thanks to my family for supporting me in my efforts to become whatever I want to be.

Funding for this research was provided by the National Science Foundation Office of Polar Programs grant OPP-0229305 to Phil Kyle (Principal Investigator). Travel to IAVCEI General Assembly 2004 was provided by the New Mexico Tech Grad Student Association.

The observatory worker, who has lived a quarter of a century with Hawaiian lavas frothing in action, cannot fail to realize that gas chemistry is the heart of the volcano magma problem.

T.A. Jaggar

1. Introduction

Measuring volcanic gas emissions is a valuable tool in evaluating active processes. Sulfur dioxide (SO_2) is typically the third most abundant volcanic gas, after carbon dioxide (CO_2) and water (H_2O) (Giggenbach, 1996). This is not the case at Erebus volcano, where carbon monoxide (CO) is the third most abundant gas (Wardell et al., 2004). CO_2 and H_2O have large atmospheric concentrations that make emission rate measurements difficult and often imprecise (Wardell et al., 2004). Low ambient atmospheric concentrations of SO_2 and an ultra violet (UV) absorption cross section allows volcanic SO_2 emission rates to be readily measured (McGonigle and Oppenheimer, 2003). SO_2 emission rate determinations provide insight into magmatic properties and degassing behavior. These properties include total magma volume degassed over a given time frame and total volatile budget for a system (Rose et al., 1982; Gerlach and Graeber, 1985; Daag et al., 1996). Moreover, Daag et al. (1996) presented an eruption prediction model based on SO_2 emission rate data collected during routine surveillance prior to the 1991 Mt. Pinatubo eruption. SO_2 emission rates are also a tool used to determine other volcanic gas and aerosol (e.g. HF, HCl, trace metals) emission rates via volatile ratios (Zreda-Gostynska et al., 1993, 1997).

The correlation spectrometer (COSPEC) was originally developed to measure SO_2 emission rates from industrial smoke stacks (Moffat and Millan, 1971). During the early 1970s, it became the dominant instrument used for volcanic SO_2 emission rate

measurements (Stoiber et al., 1983). COSPEC is now being replaced by a smaller, cheaper ultraviolet differential optical absorption spectrometer (DOAS). DOAS has been shown to be equally effective at measuring SO_2 emission rates as COSPEC (Galle et al., 2002). DOAS is now finding widespread uses on many volcanoes (Oppenheimer et al., 2004; Elias et al., 2006).

The objectives of this study at Erebus volcano were: (1) to report SO_2 emission rates between 1992 and 2005; (2) to establish an overall SO_2 budget; (3) to compare and contrast the COSPEC and DOAS collection methods at a low SO_2 emission rate volcano; and (4) to model emission rate trends in relation to volcanic degassing and lava lake convection.

2. Background

2.1 Mt. Erebus Volcano

Mt. Erebus is a large (3794 m, 1800km^3) active, alkaline, intraplate stratovolcano that forms the bulk of Ross Island, Antarctica (77º32' S, 167º10'E) (Fig. 1). The volcano contains a Main Crater, approximately 600 m in diameter, and also a smaller Inner Crater which is ~250 m in diameter. A persistent, convecting, passively degassing, phonolite lava lake, first observed in 1972 and probably present earlier, is located in the Inner Crater approximately 100 m below the Main Crater floor and 220 m below the Main Crater rim (Giggenbach et al., 1973; Kyle et al., 1982). Werner Vent is another active vent located within the Inner Crater, west of the Main Lava Lake.

Mt. Erebus lies at the southern end of the Terror Rift, a major graben within the larger Victoria Land Basin (Cooper et al., 1987; Kyle, 1990). Mantle upwelling via a large mantle plume is thought to have caused crustal thinning, rifting and subsequent volcanism in the area (Kyle and Cole, 1974; Cooper et al., 1987). Smaller volcanic centers on Ross Island include Mt Bird, Mt. Terror and multiple vents on Hut Point Peninsula, which are aligned at 120º with respect to Mt. Erebus. Previous work suggests these centers occur along radial fractures associated with crustal doming (Kyle and Cole, 1974; Kyle, 1990). As the ascending mantle plume partially melts, it provides magma for the volcanic centers located on Ross Island (Kyle et al., 1992).

Kyle et al. (1992) modeled the Mt. Erebus magmatic lineage as a basanite to phonolite sequence produced by fractional crystallization of olivine, pyroxene, feldspars, opaque oxides and apatite. Anorthoclase megacrysts, olivine, clinopyroxene, magnetite

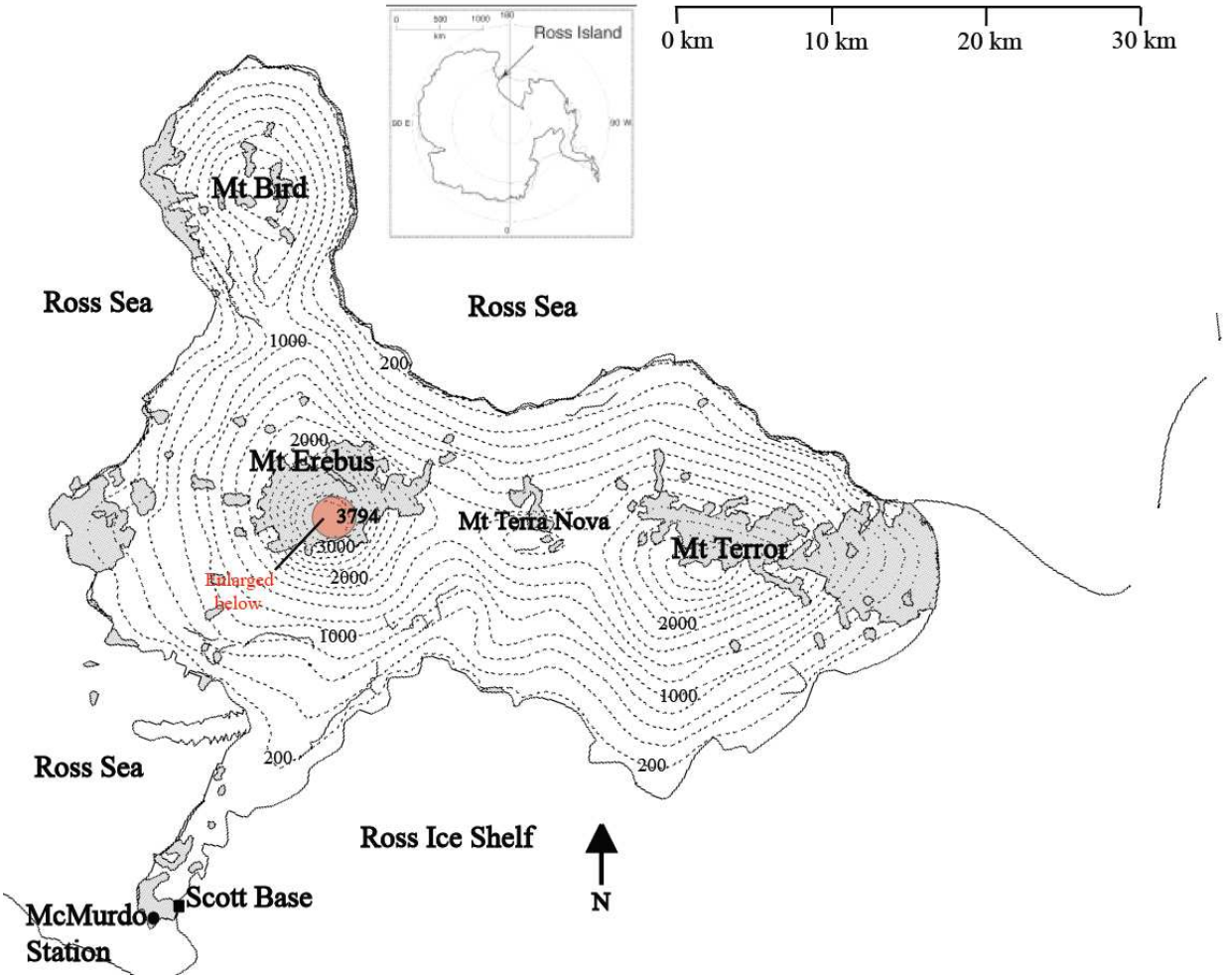

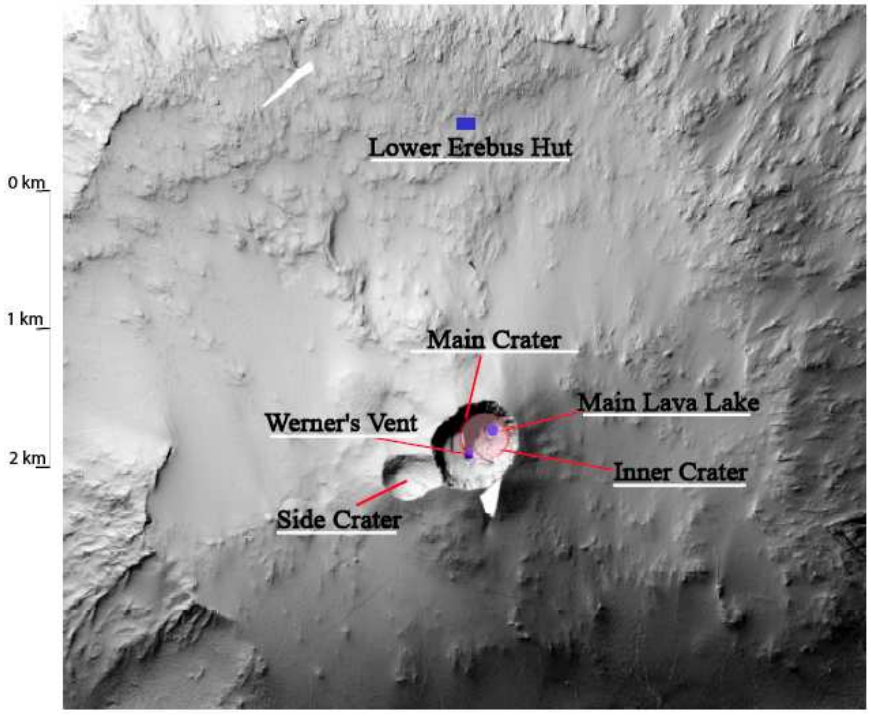

Figure 1: Location map of Mt. Erebus Volcano, Ross Island, Antarctica. After Mikelich, 2006.

and apatite constitute the modern Mt. Erebus phonolite phenocryst assemblage (Kyle et al., 1992). Esser et al. (2004) provided a timeline model for magmatic evolution based on $^{40}Ar/^{39}Ar$ dating, suggesting that magmatic differentiation occurred over approximately 1 Ma. True phonolite, which dominates the upper volcanic edifice and lava lake, did not develop until 33-26 ka ago (Esser et al., 2004; Harpel et al., 2004).

Strombolian eruptions with minor ash eruptions have characterized eruptive activity at Mt. Erebus since 1984 (Kyle et al., 1982; Kyle et al., 1992; Kyle et al., 1994; Rowe et al., 2000). Rowe et al. (2000) provides a detailed discussion on eruptions of Erebus volcano. Between 1983 and 2001, when eruption rates were elevated, the average eruption rate was zero to six eruptions per day. During increased activity in 1984, large (up to 10m) bombs were thrown over 2 km from the crater during numerous eruptions (Kyle and Meeker, 1988; Kyle et al., 1992; Kyle et al., 1994). Since 2001, the eruption rate dropped considerably to less than one eruption per week until 2005 when it increased from 0 to 6 eruptions per day.

2.2 Previous Volatile Studies

SO_2 flux measurements have been obtained at Erebus volcano on an almost yearly basis since 1983 using a COSPEC (Table 1) (Rose et al., 1985; Kyle et al., 1994). Changes in lava lake dimensions have been observed since work began in 1972 and are linked to SO_2 emission rates (Kyle et al., 1982; Kyle et al., 1994). In 1983, an average emission rate of 230 Mg/day (2.7 kg/s) was measured by Rose et al. (1985). In 1984, debris from large eruptions covered the lava lake, causing the SO_2 emission rates to drop to 25 Mg/day (0.3 kg/s). Subsequently, when the lava lake area increased, SO_2 emission

Table 1: Previous SO_2 emission rates collected by correlation spectroscopy (COSPEC).

Year	Daily flux Mg/d	N*	Reference
Dec. 1983	230±90**	27	Rose et al., 1985
Dec. 1984	25±10	41	Kyle et al., 1994
Dec. 1985	16±7	67	Kyle et al., 1994
Dec. 1986	21±11	244	Kyle et al., 1994
Dec. 1987	44±27	277	Kyle et al., 1994
Dec. 1988	27±9	941	Kyle et al., 1994
Dec. 1989	52±21	1405	Kyle et al., 1994
Jan. 1991	71±20	513	Kyle et al., 1994

*N- number of measurements
**Standard deviation is given as 1σ

rates increased to approximately 70 Mg/day (0.8 kg/s) in 1991 (Kyle et al., 1994) (Table 2).

Melt inclusions, small magma pockets trapped within crystals during growth (Roedder, 1984), have provided another tool to assess physical and chemical properties of Erebus volcano magmas (Dunbar et al., 1994; Eschenbacher, 1998). Magmatic pre-eruptive volatile contents (obtained from volatile content measurements in melt inclusions) in combination with SO_2 emission rates provide the data to determine volatile solubility, magma degassing rates and volume of degassed magma (Devine et al., 1984; Roedder, 1984; Dunbar et al., 1994; Danyushevsky et al., 2002). Melt inclusions can also be used to study crystallization processes and pre-eruptive magma chemistry. Dunbar et al. (1994) used anorthoclase hosted melt inclusions to determine S (650 ppm), H_2O (2000 ppm), Cl (1700 ppm) and F (2700 ppm) contents. Eschenbacher (1998) used electron and ion microprobes and Fourier transform infrared spectroscopy to determine pre-eruptive H_2O (1700 ppm), CO_2 (690 ppm) and S (375 ppm) contents of anorthoclase-hosted melt inclusions. Seaman et al. (2006) showed variable water ranging from 410 ppm to 3630 ppm with an average of ~1500 ppm in anorthoclase-hosted phonolite melt inclusions.

Table 2: Lava lake areas measured via remote sensing and visual observations at the crater rim.

Year	Lava Lake Area (m^2)	Reference
1980	4500	Glaze et al., 1989
		Harris et al., 1997
1983	2800	Rose et al., 1985
1984	200	Symonds et al., 1985
1985	180	Kyle et al., 1990
		Rothery and Francis, 1990
		Harris et al., 1999
1986	300	Kyle et al., 1990
1987	380	Kyle et al., 1994
1988	240	Kyle et al., 1994
1989	630	Kyle et al., 1994
	300	Harris et al., 1999
1991	650	Kyle et al., 1994
2003	2125	Davies et al., 2005
	1630	Calkins, 2006

3. Methods

3.1 Correlation Spectroscopy (COSPEC)

Sulfur dioxide (SO_2) emission rates were measured at Erebus volcano from 1983 to 2003, using a Barringer correlation spectrometer (COSPEC V) (Rose et al., 1985; Kyle et al., 1994). Light enters the COSPEC through a telescope with a 23 by 7 milliradian (mrads) field of view. After a grating diffracts the light, it passes through a spinning correlation disk containing four masks with etched slits that correspond to the peaks and troughs of the SO_2 absorption spectrum (McGonigle and Oppenheimer, 2003). These peaks and troughs occur between 300 and 315 nm, respectively, and correlate with high and low SO_2 absorption wavelengths (Stoiber et al., 1983, Millan et al., 1985). Calibrations cells were used in the determination of SO_2 emission rates by placing a cell of known SO_2 concentration in the optical path. Calibration measurements were typically collected every 15-20 minutes.

Scanning COSPEC measurements were made at the Lower Erebus hut, 2100m from the crater, as the plume rose above the crater rim (Kyle and McIntosh, 1989). The scanner was modified to allow for automatic tilt measurements, which are necessary when the plume is blown horizontally by winds. The scanner and COSPEC were interfaced to a laptop and data from each instrument were collected using an in house computer program (*COSPEC*) which recorded scan angle, scan rate and SO_2 measurement data. *ASPEC*, another in-house program, was used to calculate emission rate data.

3.2 Differential Optical Absorption Spectroscopy (DOAS)

DOAS spectrometers were used to measure SO_2 emission rates during the 2003 and 2005 field seasons. COSPEC and DOAS data were simultaneously collected in 2003, allowing for a direct comparison between the two instruments. DOAS, like COSPEC, measures the absorption of ultraviolet light to measure SO_2 concentrations. DOAS is useful for a variety of chemical species with distinct, narrow banded (~5 nm) absorption cross sections. Platt (1994) provides a detailed review of the technique.

COSPEC and DOAS differ in the gas correlation procedure during the data retrieval process (McGonigle and Oppenheimer, 2003). COSPEC correlates instantly with the spinning correlation disc, thereby limiting the data collected to a single SO_2 absorption band. DOAS collects a spectrum from 200 to 400 nm with a resolution of 0.6 nm, so multiple gas species can be measured simultaneously (Galle et al., 2002; Oppenheimer et al., 2005). Identification and measurement of SO_2 absorption (referred to as retrieval) are performed by scaling a laboratory measured spectrum to the observed spectrum (Vandaele et al., 1994; McGonigle and Oppenheimer, 2003). Figure 2 shows the SO_2 laboratory measured spectrum.

The DOAS used at Erebus volcano was similar to that described in Galle et al. (2002). Telescopes with a field of view of 8 mrads or 20 mrads were used to collect light and this was transferred to an Ocean Optics USB2000 spectrometer via a 1-3 m long fiber-optic cable. The cable consists of four 200μm diameter solarization resistant quartz fibers (Galle et al., 2002).

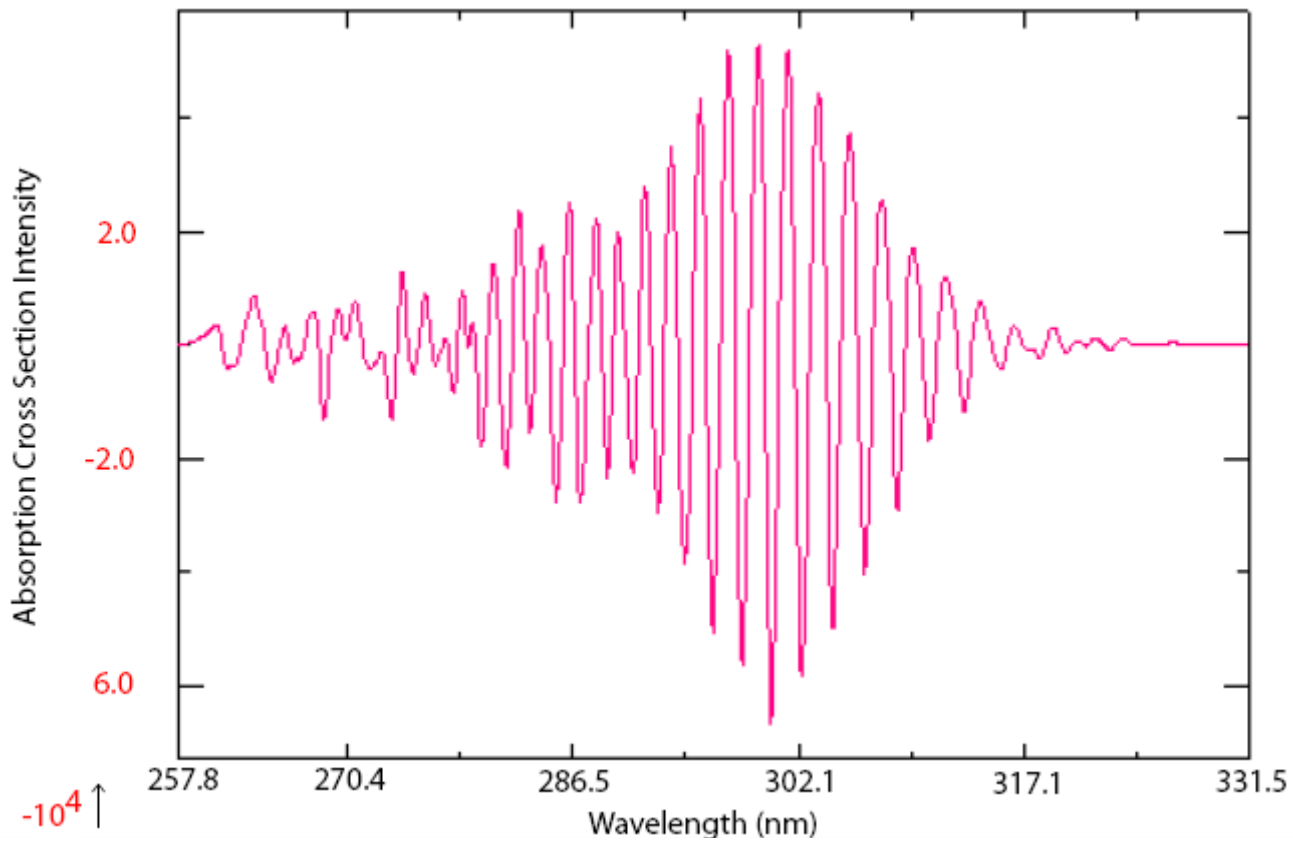

Figure 2: Laboratory measured SO_2 absorption cross section (Vandaele et al. 1994).

A laptop computer provided power to the spectrometer and collected data from the DOAS via a USB cable. *DOASIS* was used to run the spectrometer on a variety of data collection platforms including helicopter and snowmobile traverses, and stationary scans. A GPS, linked to the computer via HyperTerminal, was used to ascertain location during mobile traverses.

SO_2 concentrations were obtained through a series of mathematical manipulations of the spectra following Galle et al. (2002). Data were reduced using scripts in the *DOASIS* software. Stationary scans were reduced using *DOASFLUX*, a program written in *MATLAB* and modeled after *ASPEC*. Appendix A provides a more detailed discussion of the methods used to determine SO_2 emission rates.

Plume rise rates, the largest source of error in flux measurements, were measured by videoing the vertically rising plume (Kyle et al., 1994). When a plume rise rate was not directly obtained the rise rate was estimated from previous measurements. During horizontal traverses, wind speed measurements were collected at the crater rim with a hand-held anemometer. Appendix A discusses the plume velocity measurements in more detail.

All measurements are listed as Mg/day with kg/s in parentheses and errors are reported at $\pm 1\sigma$.

4. Results

4.1 Plume Velocities

Plume velocity measurements constitute the largest source of error in flux measurements due to the difficulty in measuring this parameter (Stoiber et al., 1983; McGonigle et al., 2005). Virtually all COSPEC and DOAS emission rate measurements were obtained from a vertically rising plume, which is driven by thermal gradients in emissions from the lava lake and fumaroles. During COSPEC and DOAS data collection, the vertically rising plume was videoed and later played back to determine the rise rates. Typically, plume rise rate measurements were obtained once every two minutes for the duration of COSPEC and selected DOAS data collection. Table 3 shows the average measured plume rise rate obtained between 1996 and 2003. Over 1200 measurements yielded an average plume rise rate of 4.6 ± 1.7 m/s. Plume velocities were correlated to specific datasets using timestamps collected with the rise rate measurement. When a plume rise rate was unavailable, a rate of 5 ± 1 m/s was assumed based on the time-averaged value obtained since monitoring began in 1983.

4.2 Calibrations

Calibrations were collected periodically during COSPEC data acquisition. These were then averaged and used to convert the COSPEC signal (volts) to ppm m. Ultraviolet light intensity changed throughout the day, which affected calibrations. In addition to calibration, the COSPEC outputs automatic gain control (AGC), a measure of instrumental amplification in response to UV changes. AGC can also be used to monitor

Table 3: Average daily plume rise rates measured from video records of the plume.

Year	Date	N*	Average Plume Rise Rate m/s	SD**
1996	8 Dec	60	3.8	1.3
	9 Dec	54	3.4	1.1
1997	6 Dec	57	2.0	0.6
	15 Dec	59	3.6	1.1
2000	8 Dec	74	3.9	1.5
	10 Dec	57	3.3	1.0
	13 Dec	34	3.7	1.1
	14 Dec	85	4.1	1.7
2001	1 Dec	151	5.6	1.7
	2 Dec	101	5.2	1.2
	3 Dec	20	3.5	1.1
2003	6 Dec	16	3.7	0.8
	11 Dec	444	5.6	1.4
TOTAL		**1258**	**4.6**	**1.7**

* N- number of measurements
** SD- Standard deviation

instrument noise throughout the day. Figure 3 shows the variation in both AGC and calibration with changing light levels measured throughout a day. AGC and calibration data are inversely related. Typically, calibration data does not change appreciably during a sequence of measurements, therefore measuring calibrations before and after each COSPEC peak scan is not necessary.

4.3 Plume Width

Plume width was calculated from the peak width on the data trace. The plume width was determined from following equation:

$$W_p = 2*[\tan ((PT/2)*SR)*D] \quad (1)$$

W_p is plume width (m), SR is scan rate (degrees/second), D is distance to the plume (m), and PT is the scan time across the observed SO_2-bearing plume (seconds). Peak times were determined by cross referencing the data trace with the plume video and selecting data points representative of the plume boundaries. Throughout the day, plume widths and visibility varied greatly due to changing atmospheric conditions such as humidity, wind velocity and cloud cover. Wide plumes ranged from 400 to 600 m (Fig. 4a), whereas narrow plumes measured between 200 and 400 m (Fig. 4b).

For horizontal scans across a vertically rising plume, SO_2 emission rates were measuring using:

$$Emission\ Rate = \cos\theta * B * W_p * RR_p * 0.00023 \quad (2)$$

where cos θ accounts for the difference between COSPEC tilt and the horizontal plane, B is burden (ppm m) measured by COSPEC and DOAS, W_p is the plume width (m), RRp is the plume rise rate (m/s) and 0.00023 is a conversion factor. A more detailed discussion

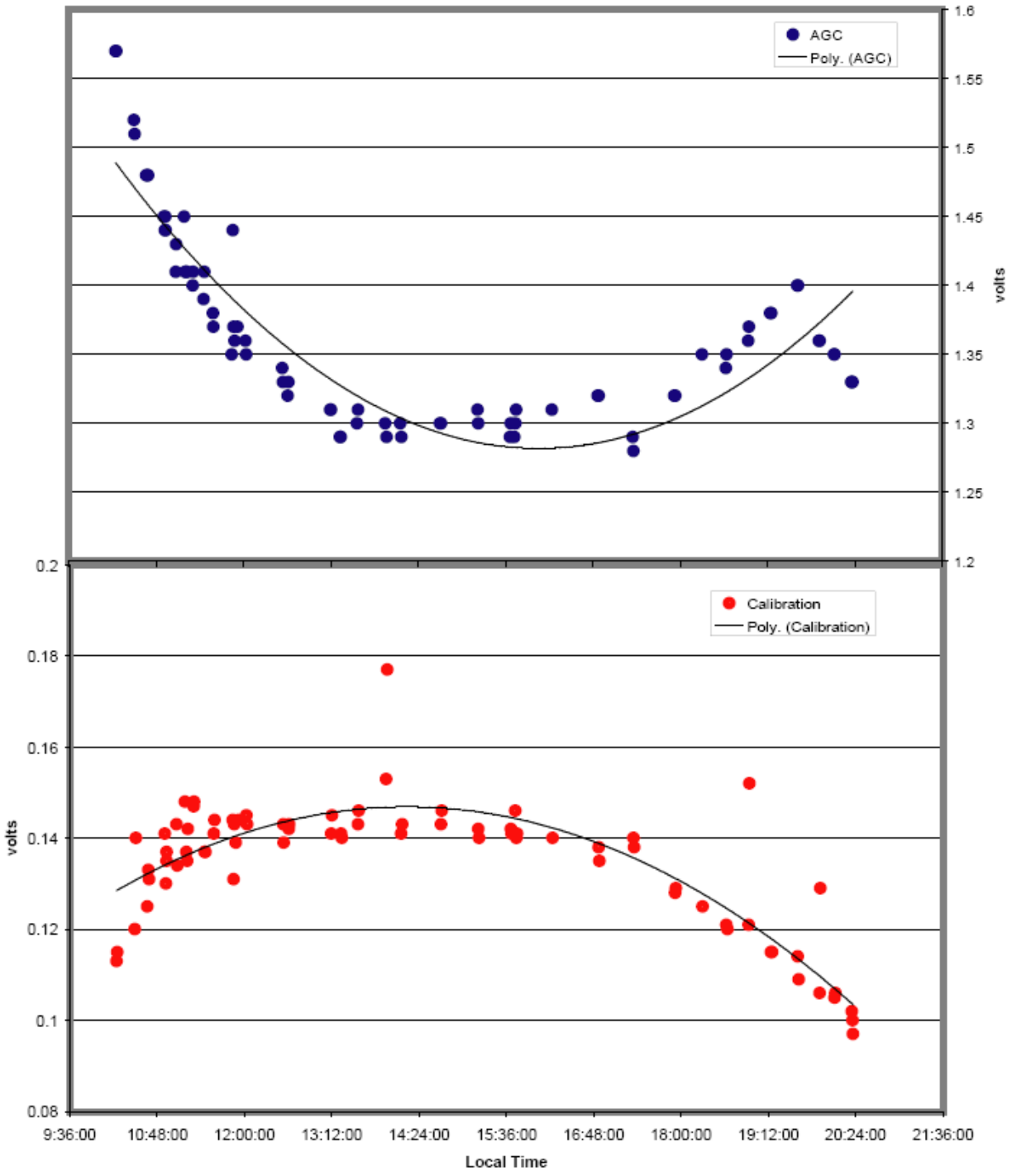

Figure 3: Representative calibration and automatic gain control curves versus time. The poly curve shows the general data trend over the course of the day. The automatic gain control is the inverse of the calibration curve.

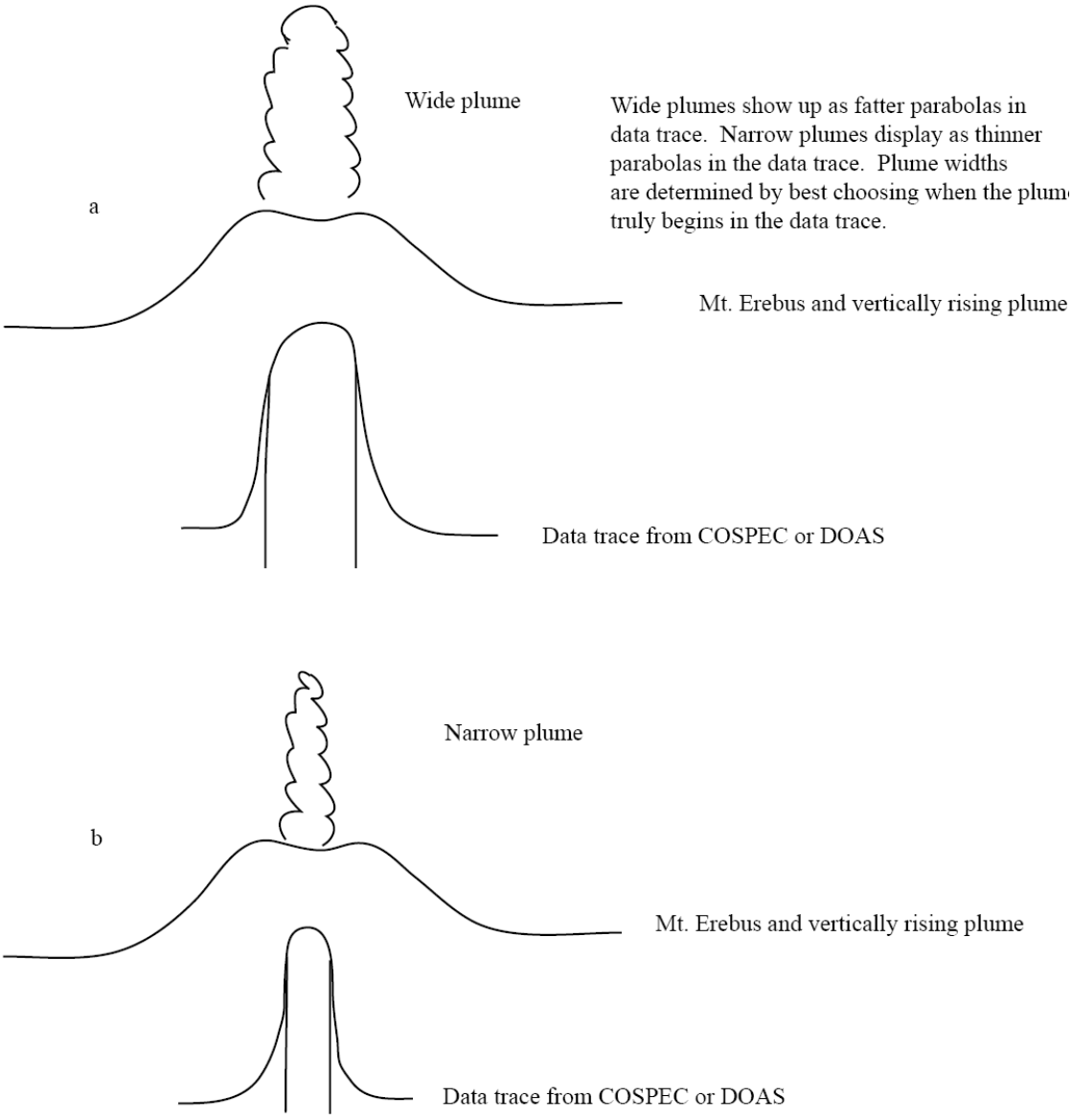

Figure 4: Schematic of ideal plume as it rises above the crater rim and recorded on a data trace. a) Wide plumes will have wider data traces and "windows" of where the user identifies the data points where the plume begins and ends. b) Narrow plumes will have thin data traces. The procedure by which a user chooses a "window", i.e. deciding when the plume begins and ends on the trace, is the same for narrow plumes.

of this equation is in Appendix A. All other parameters being equal, large plume widths yield larger emission rates while smaller plume widths give smaller emission rates. The scanner was positioned to collect SO_2 emission data directly above the crater rim. The crater of Erebus volcano is ~600 m in diameter, therefore measured plume widths should typically be less than 600 m. This was used as an internal check of each emission rate measurement. Measurements with an apparent plume width >600 m were re-examined and the video record consulted. In some cases, the data were recalculated with a narrower plume width.

The sampling frequencies for DOAS and COSPEC were different and affected the plume width estimates. COSPEC measurements were made every 1 second, whereas DOAS measurements were made every 1-3 seconds. The lower sampling frequency for the DOAS subsequently biases the user toward smaller plume widths and therefore smaller SO_2 emission rate (Fig. 5).

4.4 COSPEC

COSPEC was the primary method to obtain SO_2 emission rate rates at Erebus volcano since 1983. Data collected between 1983 and 1991 is presented in Kyle et al. (1994). Data collected between 1992 and 2001 were collected by P. Kyle. Since 1992, over 7000 individual SO_2 emission rate measurements have been retrieved by COSPEC. Typically, data was collected over several days during the first three weeks of December, weather permitting. Table 4 shows the daily averages acquired between 1992 and 2003. Individual measurements fluctuated widely throughout the day (Fig. 6). The lowest individual emission rate collected was 0.3 Mg/day (0.004 kg/s) and the highest was 175

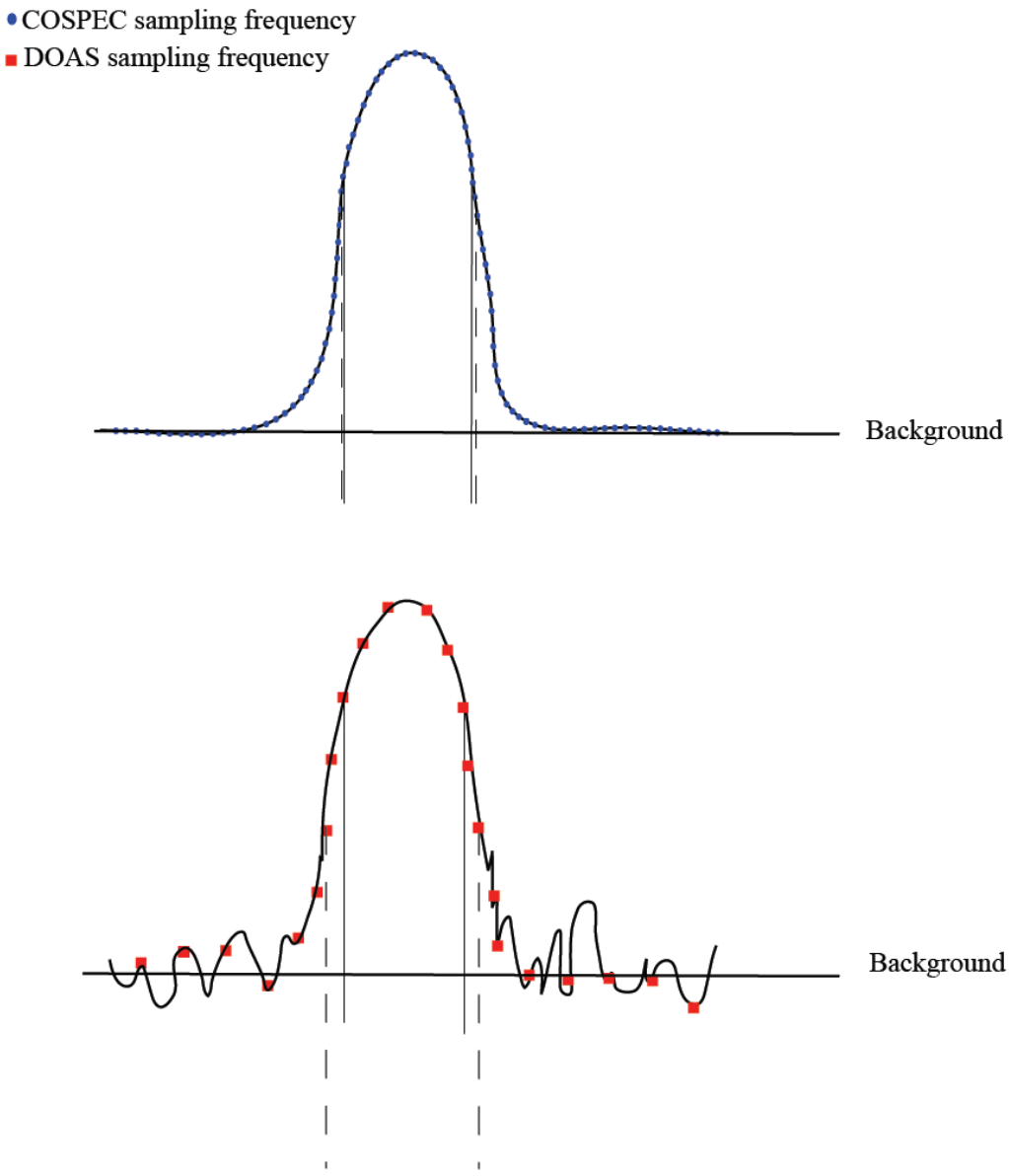

Figure 5: Cartoon of plume showing sampling frequency for COSPEC and DOAS. The differences in plume traces indicate relative background noise for each instrument. COSPEC background noise is quieter than DOAS background noise. The solid and dashed lines show two different options for the plume width. With the COSPEC data, the difference between the dashed and solid lines does not affect the plume width. With the DOAS data, the difference between the dashed and solid lines is larger and does affect the plume width output.

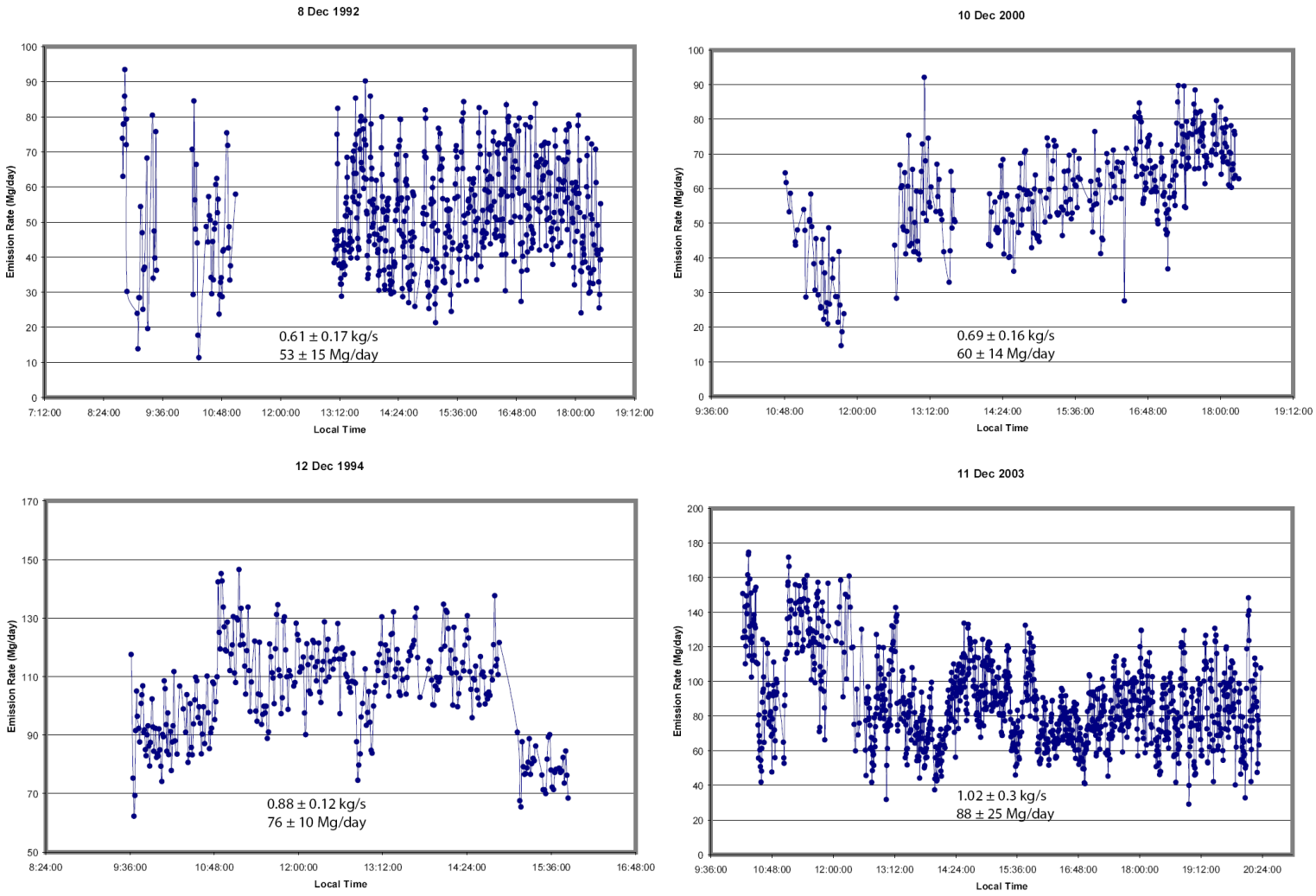

Figure 6: Four representative examples of daily SO_2 emission rates from Erebus volcano collected between 1992 and 2003. Note the different scales on each graph. Fluctuations persist strongly in all four days and range from a factor of 2 to a factor of 9. Emission rate trends include: steady increases (10 Dec 2000), increases then decreases (12 Dec 1994), slight decreases (11 Dec 2003) and relatively stable emissions with large variability (8 Dec 1992).

Table 4: Daily averaged SO_2 emission rates measured by COSPEC at Mt. Erebus volcano between 1992 and 2003.

Year	Date	Local Time	N*	Low Flux	High Flux	Average Daily Flux Mg/day (kg/s)	SD**
1992	6-Dec	8:20-13:55	146	15.4	61.2	36 (0.42)	9 (0.10)
	8-Dec	8:45-18:30	582	11.3	93.4	53 (0.61)	15 (0.17)
	17-Dec	10:05-10:37	36	18.7	63.3	36 (0.42)	13 (0.15)
	18-Dec	20:05-20:50	53	56.5	93.5	73 (0.84)	7 (0.08)
	21-Dec	8:30-10:25	114	33.3	99.1	62 (0.72)	12 (0.14)
1993	6-Dec	15:20-17:45	147	52.5	78.8	62 (0.72)	5 (0.06)
	7-Dec	13:50-17:55	145	13.8	55.3	30 (0.35)	7 (0.08)
	8-Dec	12:00-14:55	188	30.6	65.8	42 (0.49)	5 (0.06)
	12-Dec	8:50-18:50	511	13.2	84.8	38 (0.44)	12 (0.14)
	13-Dec	10:40-11:25	29	38.5	115	87 (1.01)	18 (0.21)
1994	7-Dec	9:25-11:20	20	40.3	68.8	54 (0.63)	8 (0.09)
	10-Dec	8:55-11:00	65	25.9	95.6	55 (0.64)	15 (0.17)
	12-Dec	9:35-15:50	336	62.2	147	76 (0.88)	10 (0.12)
1996	8-Dec	18:20-20:54	73	15.1	47.7	28 (0.32)	6 (0.07)
	9-Dec	14:28-14:47	30	21.1	47.3	32 (0.37)	7 (0.08)
	10-Dec	9:57-20:33	296	19.1	99.8	48 (0.56)	13 (0.15)
	11-Dec	9:12-14:57	364	0.5	72.7	38 (0.44)	18 (0.21)
1997	6-Dec	18:42-20:36	144	10.7	27.2	17 (0.20)	3 (0.03)
	15-Dec	13:03-19:08	283	25.6	95.8	60 (0.69)	13 (0.15)
2000	8-Dec	9:31-15:49	87	25.6	90.6	47 (0.54)	13 (0.15)
	10-Dec	10:48-18:18	356	14.6	92.1	60 (0.69)	14 (0.16)
	12-Dec	9:14-16:51	273	28	70.6	49 (0.57)	8 (0.09)
	14-Dec	11:38-16:14	383	0.3	116	62 (0.72)	24 (0.28)
2001	1-Dec	10:44-18:12	597	31.4	102	52 (0.60)	13 (0.15)
	2-Dec	9:49-13:20	357	16.5	82.7	48 (0.56)	11 (0.13)
	3-Dec	14:34-18:28	161	19.1	109	70 (0.81)	28 (0.32)
2003	6-Dec	8:44-11:30	239	38.1	109	68 (0.79)	14 (0.16)
	11-Dec	10:13-20:22	1195	29	175	88 (1.02)	25 (0.29)

* N- number of measurements
** SD- Standard deviation

Mg/day (2.0 kg/s), both in 2003. Such variation has been noted since monitoring began in 1983 (Kyle et al., 1994). All individual measurements in a single day were averaged to obtain a daily average. Daily averages ranged from 17±3 Mg/day (0.2 kg/s) in 1997 to 88±25 Mg/day (1 kg/s) in 2003.

Daily averages from at least two days of measurements collected in a single year were analyzed for variability and then averaged to give an annual emission rate (Fig. 7) (Table 5). Averaging dampens the signal even more, but this is used to provide a conservative estimate of an annual average emission rate. Average emission rates began at 52±16 Mg/day (0.6 kg/s) in 1992 then they dipped to 39±17 Mg/day (0.5 kg/s) in 1996 and increased to a high of 85±25 Mg/day (1.0 kg/s) in 2003. These rates show an SO_2 emission rate increase by a factor of two between 1996 and 2003. Yet the annual average emission rates are similar if the data is considered with the 1σ standard deviation as shown in Fig. 6. Previously collected data displayed in Table 1 show similar behavior in the emission rate data and associated 1σ. Rose et al. (1985) noted that stable lava lake activity began in 1974 and continued until 1984. The data presented here suggests that the emission rates show small yearly fluctuations, but when compared to volcanic emission rate variations elsewhere (Andres and Kasgnoc, 1997), emission rates from Erebus volcano are relatively stable.

4.5 DOAS

SO_2 emission rate measurements were collected using DOAS in 2003 and 2005 (Table 6). Data were collected in December of 2003 and 2005 and a total of 855 observations were made. No measurements were made in 2004. Appendix B provides

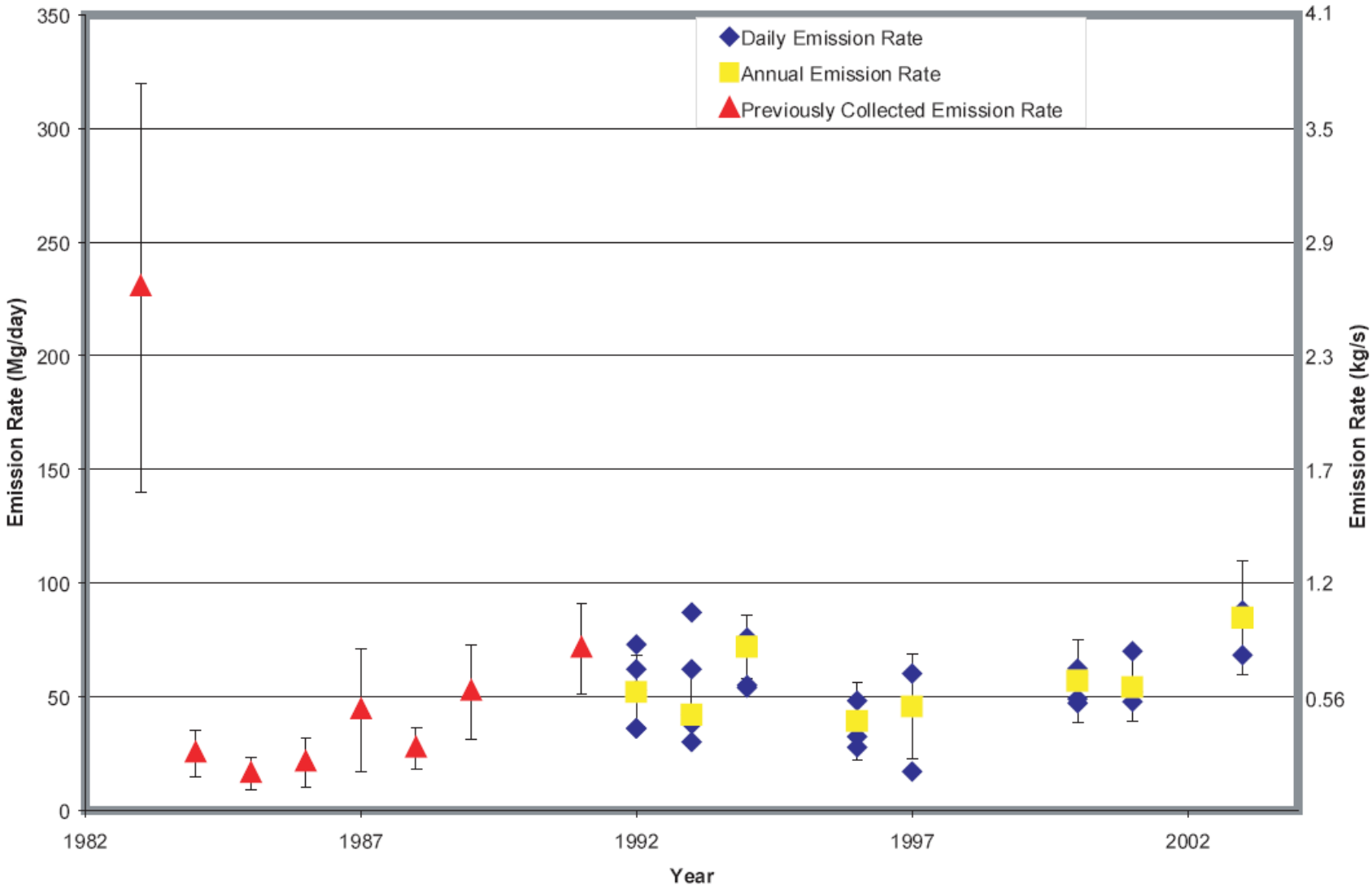

Figure 7: Average daily and average annual emission rates collected with COSPEC between 1992 and 2003. Previously collected data are shown in red triangles. Standard deviations are denoted with error bars on the annual emission rates. Overall, there is a general increase in SO_2 emission rates between 1992 and 2003. Place in context of previously collected data, the emission rates are continuing to rise after the large eruptions in 1984.

Table 5: Average annual SO_2 emission rates measured at Erebus volcano between 1992 and 2003 by COSPEC.

Year	N*	Average Annual Flux (Mg/day)	SD**
1992	931	52	16
1993	1020	42	16
1994	421	72	14
1996	763	39	17
1997	427	46	23
2000	1099	57	18
2001	1115	54	15
2003	1434	85	25

* N- number of measurements
** SD- Standard deviation

all the individual COSPEC and DOAS measurements in tabular format on a compact disc.

In 2003, data were collected on 6, 7 and 11 December. Data were collected with stationary horizontal scans as well as snowmobile and helicopter traverses under the plume. One snowmobile traverse on 6 December yielded a flux of 26 Mg/day (0.3 kg/s). Four snowmobile traverses collected on 7 December averaged 20 ± 5 Mg/day (0.2 kg/s). On 11 December 2003, helicopter traverses yielded an average of 74 ± 17 Mg/day (0.9 kg/s), based on 13 measurements (Oppenheimer et al., 2005). On the same day, horizontal scans made simultaneously with COSPEC scans gave SO_2 emission rates of 95 ± 31 Mg/day (1 kg/s).

DOAS SO_2 emission rate data collected in 2005 are similar, within 1σ, to emission rate data from 2003, despite an increase in eruptive activity. Horizontal DOAS scans, obtained over two days, averaged 76±27 Mg/day (0.8 kg/s), based on 815 measurements. Video data were not available during data reduction. Consequently, the assumed plume rise rate was 5 m/s. SO_2 emission rates were collected immediately following two eruptions, which were approximately ten minutes apart. The eruptions registered 0.4 Pa (the infrasound measurement used for eruptions) and 33.1 Pa. The respective flux rates were 39 Mg/day (0.5 kg/s) and 51 Mg/day (0.6 kg/s). There was only one SO_2 emission rate measurement associated with each eruption so standard deviations are not available.

5. Data Quality

SO_2 emission rates from Erebus volcano are inherently variable. Fluctuations make it difficult to discern real trends in the data. For the DOAS measurements, the low SO_2 emissions from Erebus volcano yields larger signal to noise ratios, which creates difficulties during data analysis. Variables like plume velocity, wind speed, UV levels and cloud cover can affect emission rates. One of the most important parameters is plume velocity. Hand-held anemometer measurements of plume velocities can contribute ±30% error in the SO_2 emission rate determination (Stoiber et al., 1983; Kyle et al., 1994). Plume velocities measured by using video recordings reduced the error from ±30% to ±5% (Kyle et al., 1994). Wind can affect plume geometry by dispersing it and causing it to fold back in on itself. The measured plume width, plume shape and SO_2 distribution across the plume can be used to identify and assess the problematic data (Kyle et al., 1996) (Fig. 8). An ideal vertically rising plume should appear symmetrical in scans across the peak. When asymmetrical peaks were observed these were cross checked against video observations to determine a physical reason for asymmetry. For example, degassing of SO_2 from Werner vent can affect the recorded peak shape (Fig. 9). If the peak shape could not be explained with physical observations, it was discarded from the data retrieval.

Gerlach (2003) discusses a potential effect of atmospheric pressure which could cause underestimation of COSPEC measurements of plume SO_2 concentrations at high elevations. He identifies what he considers to be a fundamental problem with calibration cells related to their fabrication at standard temperatures and pressures. The COSPEC

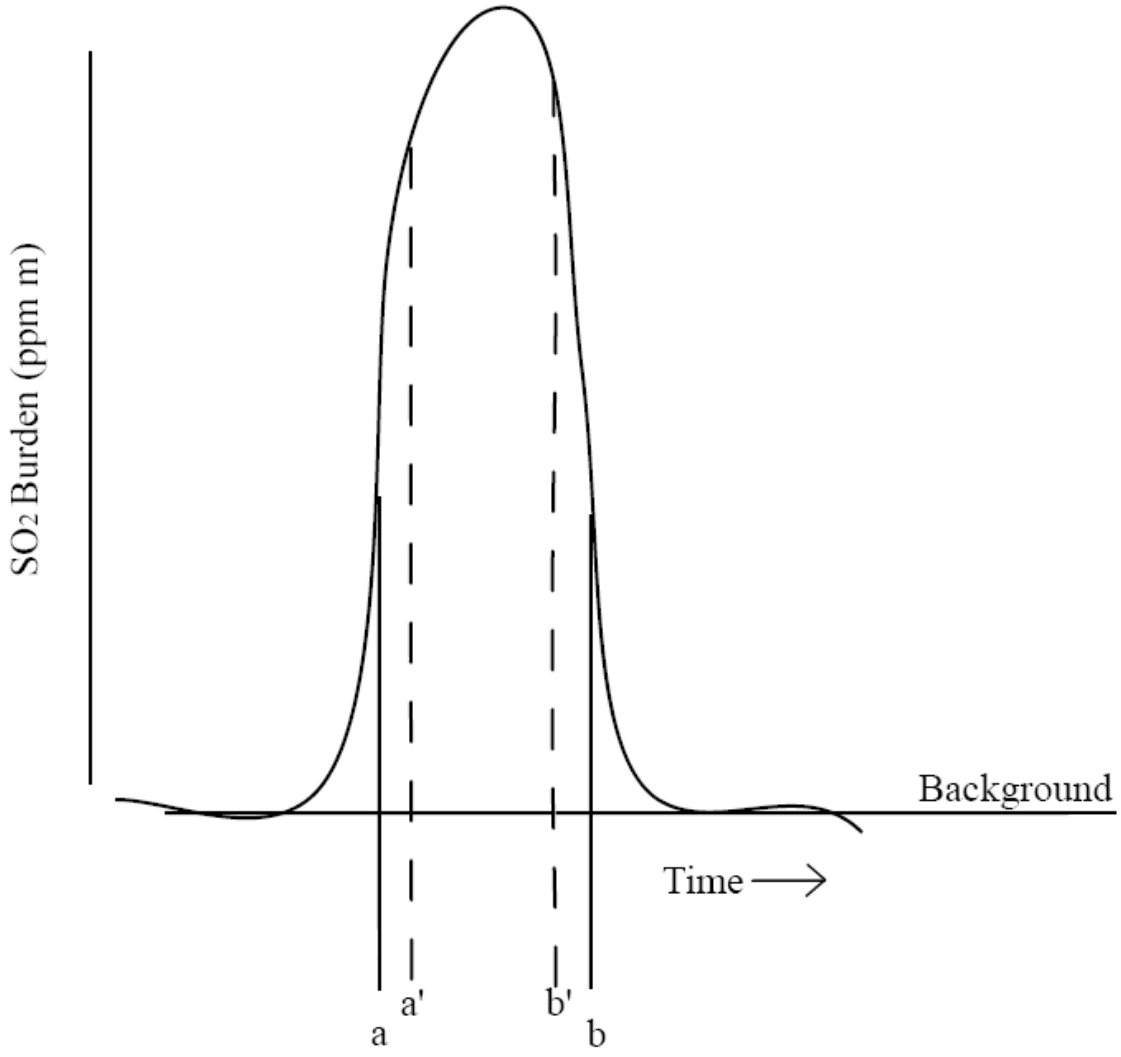

Figure 8: Idealized horizontal scan across a perfect vertically rising plume showing SO_2 burden. The center of the plume represents the maximum SO_2 concentration. The solid and dashed lines represent potential plume boundaries chosen by a user. The area under the curve is integrated and multiplied by plume velocity and width to achieve an emission rate.

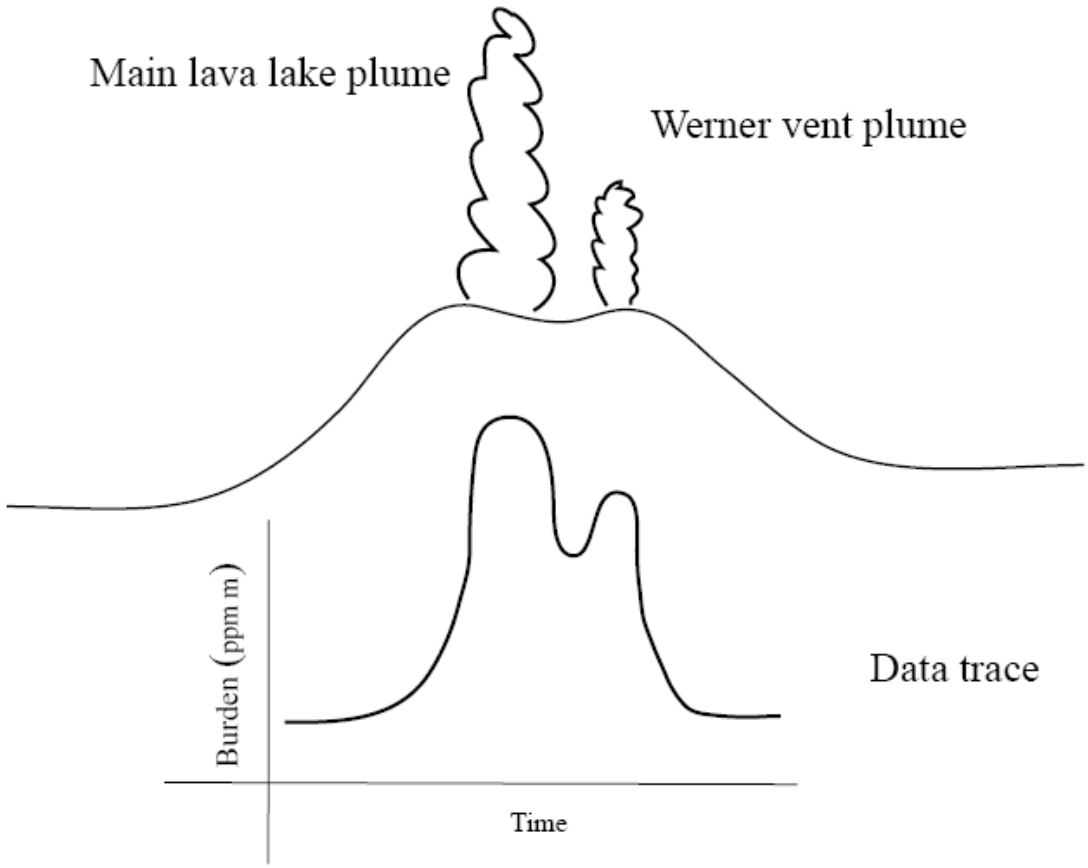

Figure 9: Idealized horizontal scan through two plumes which are occasionally observed at Erebus volcano in the past. The larger plume is emitted from the Main lava lake while the smaller plume originates from Werner vent. A diagramatic data trace is shown below the cartoon of the crater. The recording of the main plume will appear wider than the trace from Werner.

emission rates presented in this study do not need correcting for this effect. Gerlach's concern relates to SO_2 concentrations in the plume and does not affect the emission rate calculations. Emission rates collected from Mt. Erebus are typically collected at ~ -25° C and 630±10 bars. The conversion factor, 0.00023 in equation 1 (page 76) takes into account the density of SO_2 in air. It represents the number of SO_2 molecules in a given volume and is independent of temperature and pressure. This conversion factor converts temperature/pressure dependent SO_2 path-length concentrations (ppm m) to fluxes in kilograms (kg), which are temperature and pressure independent.

Calibration cells have been known to leak (McGonigle and Oppenheimer, 2003), which can make the calibration of the COSPEC impossible. We checked our calibration cells for leaks periodically. The calibration cells were also measured with the DOAS to ensure there were no leaks.

UV radiation intensity affects the remote sensing of SO_2 emissions rates collected by COSPEC and DOAS. Clouds and aerosols scatter incoming indirect sunlight increasing background UV to the point where detector saturation occurs in DOAS instrument. Saturation greatly impairs the instruments ability to detect SO_2 absorption (Oppenheimer, pers. comm.). Adjusting the coadds (number of averaged spectra per sample step) and integration time for local light levels helps mitigate these problems. High UV levels require fewer coadds and longer integration times to collect quality spectra, whereas low UV levels require more coadds and shorter integration times to acquire the best spectra. Moreover, the number of coadds directly affects data quality, because the square root of the number of coadded spectra is proportional to signal to noise ratios (Elias et al., 2006).

Several factors may explain the emission rate discrepancy between snowmobile and stationary scans. During a traverse/scan the telescope should remain perpendicular to the ground to collect the appropriate plume cross section. Crossing sastrugi (wind carved snow) fields during a traverse created an unstable platform for the telescope, causing it to lose perpendicularity. When this occurs the telescope may point outside the plume (no SO_2 molecules), toward another part of the plume with a different SO_2 concentration, or even toward the sun, affecting the SO_2 concentration retrieval. Moreover, the plume width may be larger than the effective snowmobile trail, causing the traverse to be cut off in before reaching the outer edge of the plume whereas stationary scan do reach background on both sides of the plume (Fig. 10a, 10b). This would yield a smaller SO_2 emission rate In addition to platform stability, snowmobile traverse take more time to complete one measurement. Because of these problems, snowmobile traverses should be considered a last resort.

6. Sulfur Speciation

H_2S, SO_2, H_2SO_4 and minor amounts of sulfate aerosols constitute the sulfur species emitted as a gas from volcanic systems (Symonds et al., 1994; Giggenbach, 1996). Erebus volcano magmas are reduced (Kyle, 1977), thus H_2S should be the dominant magmatic sulfur species (Rose et al., 1985; Wardell et al., 2004; Kelly, 2006). It is assumed that H_2S oxidizes to SO_2 by combustion at the lava lake-atmosphere interface. As H_2S cannot be remotely measured by COSPEC or DOAS, SO_2 is the only readily measurable S gas species on Mt. Erebus (Kyle et al., 1994).

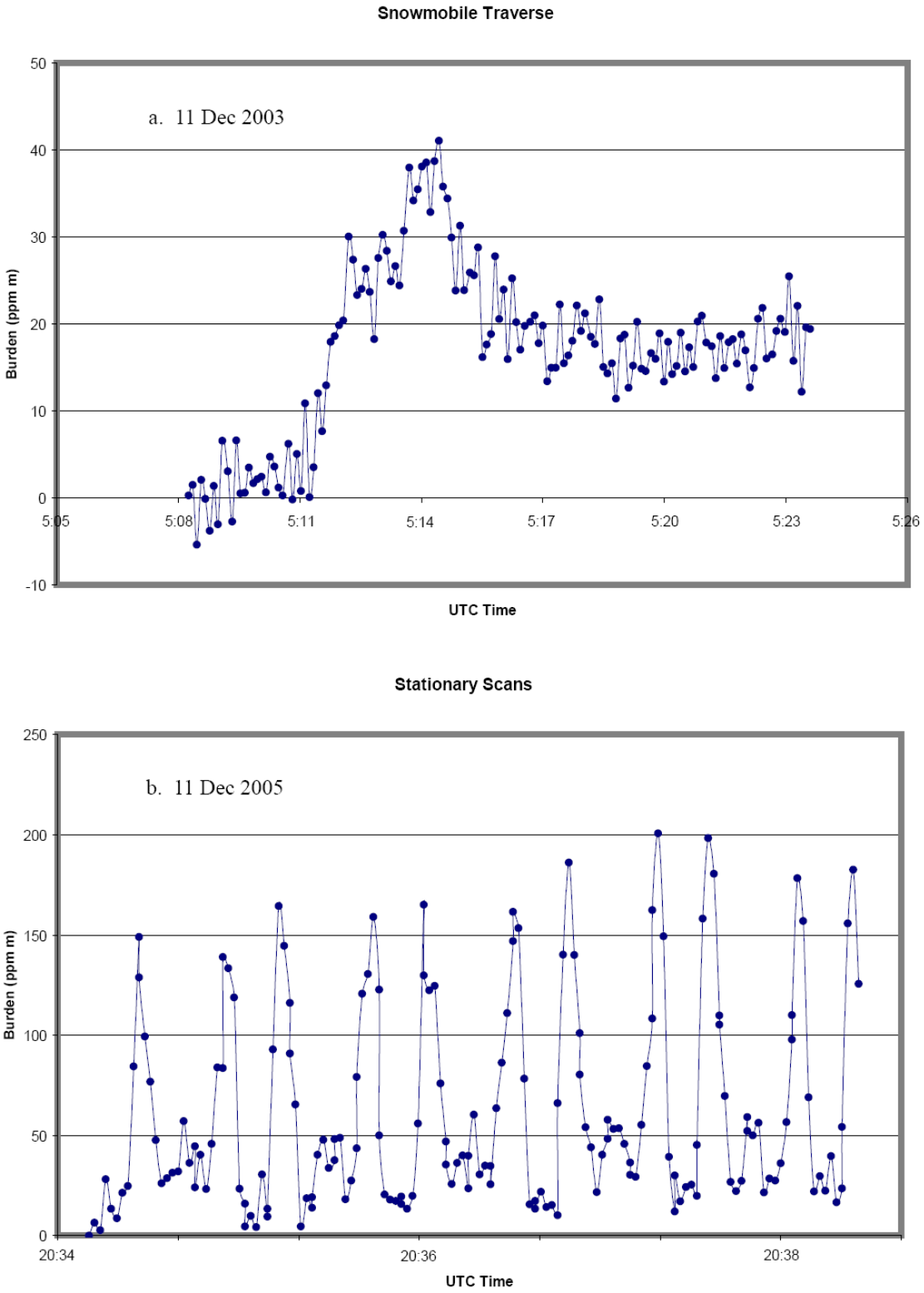

Figure 10: a) One DOAS snowmobile traverse. One measurement was obtained in approximately 15 minutes. The traverse never reached the outside of the plume. b) DOAS stationary horizontal scans. Eleven measurements were obtained in approximately five minutes and the scans were able to measure the background on both sides of the plume.

7. Comparison of COSPEC and DOAS Techniques

Simultaneous horizontal scans using COSPEC and DOAS were collected on 11 December 2003. Measured peaks suggest a good comparison between the two instruments (Fig. 11). There was also a good correlation between the burdens measured by COSPEC and DOAS (Fig. 12).

The difference between the COSPEC and DOAS burdens may be due to several factors like noisy backgrounds and telescope field of view. DOAS data are affected by noisier backgrounds, compared to COSPEC. Noisier DOAS signals were also documented during a comparison of COSPEC and FLYSPEC (flyweight DOAS spectrometer) on Kilauea (Elias et al., 2006). DOAS emission rates were lower than the COSPEC emission rates on average. Noisier signals make it more difficult to determine the background affecting the emission rate output, biasing the data toward lower emission rates. The telescope field of view area may also affect emission rate measurements. The DOAS used on Erebus volcano had a telescope with a smaller field of view than the COSPEC, reducing the light collected by the detector, ultimately increasing the signal to noise ratio (Elias et al., 2006). In general, DOAS compares adequately to COSPEC (~10% difference) when appropriate parameters are closely monitored and carefully selected to optimize data collection. While this difference is within the typical standard deviation observed in the COSPEC data, the COSPEC performs more consistently than the DOAS on Erebus volcano due to the high signal to noise ratio in the DOAS data.

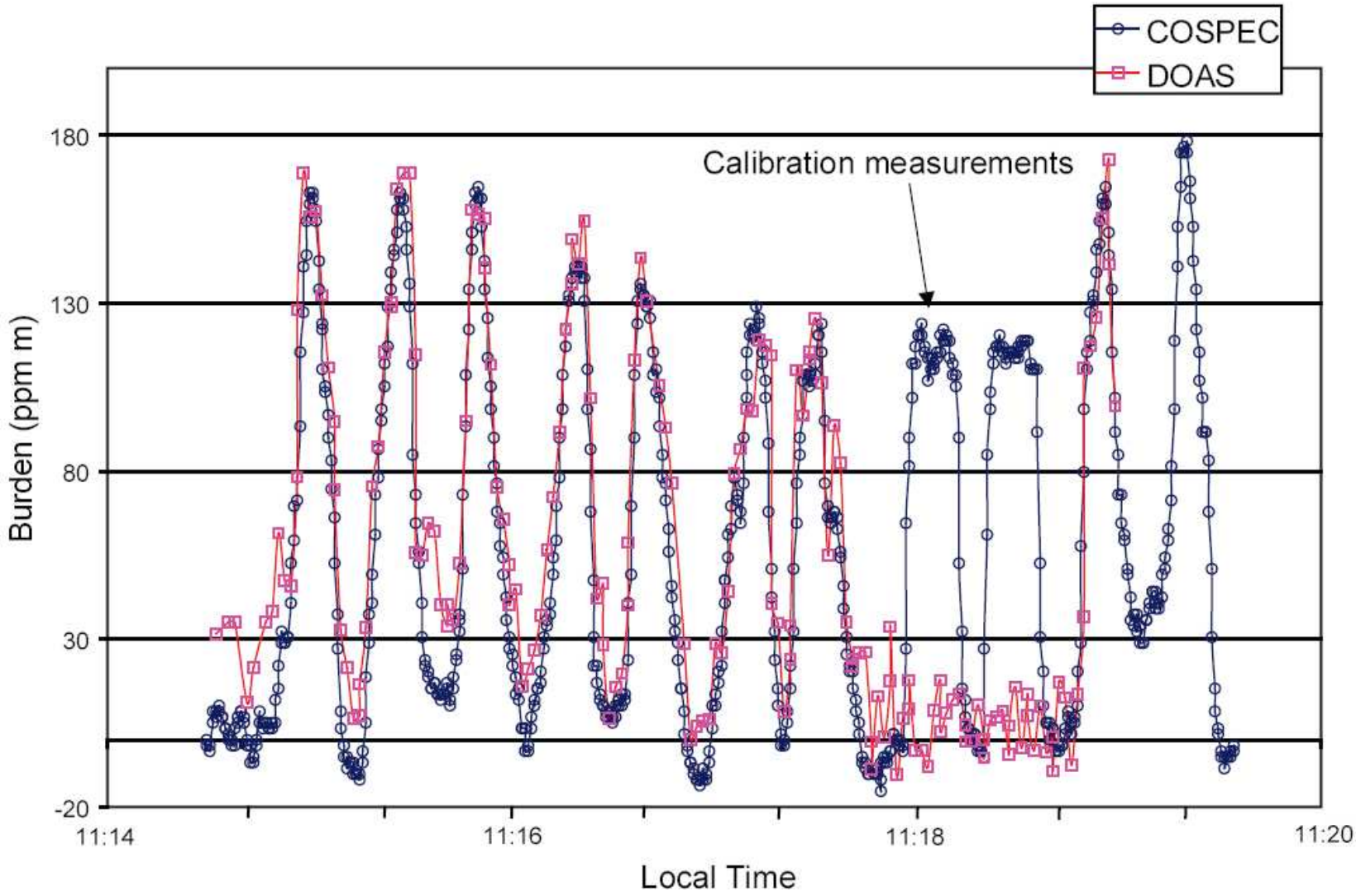

Figure 11: Simultaneous COSPEC and DOAS measurements of SO_2 burden (ppm m) versus time collected on 11 December 2003. The COSPEC and DOAS peaks correspond well with slight variations at lower concentrations possibly due to telescope field of view, signal to noise ratio and overall instrument sensitivity.

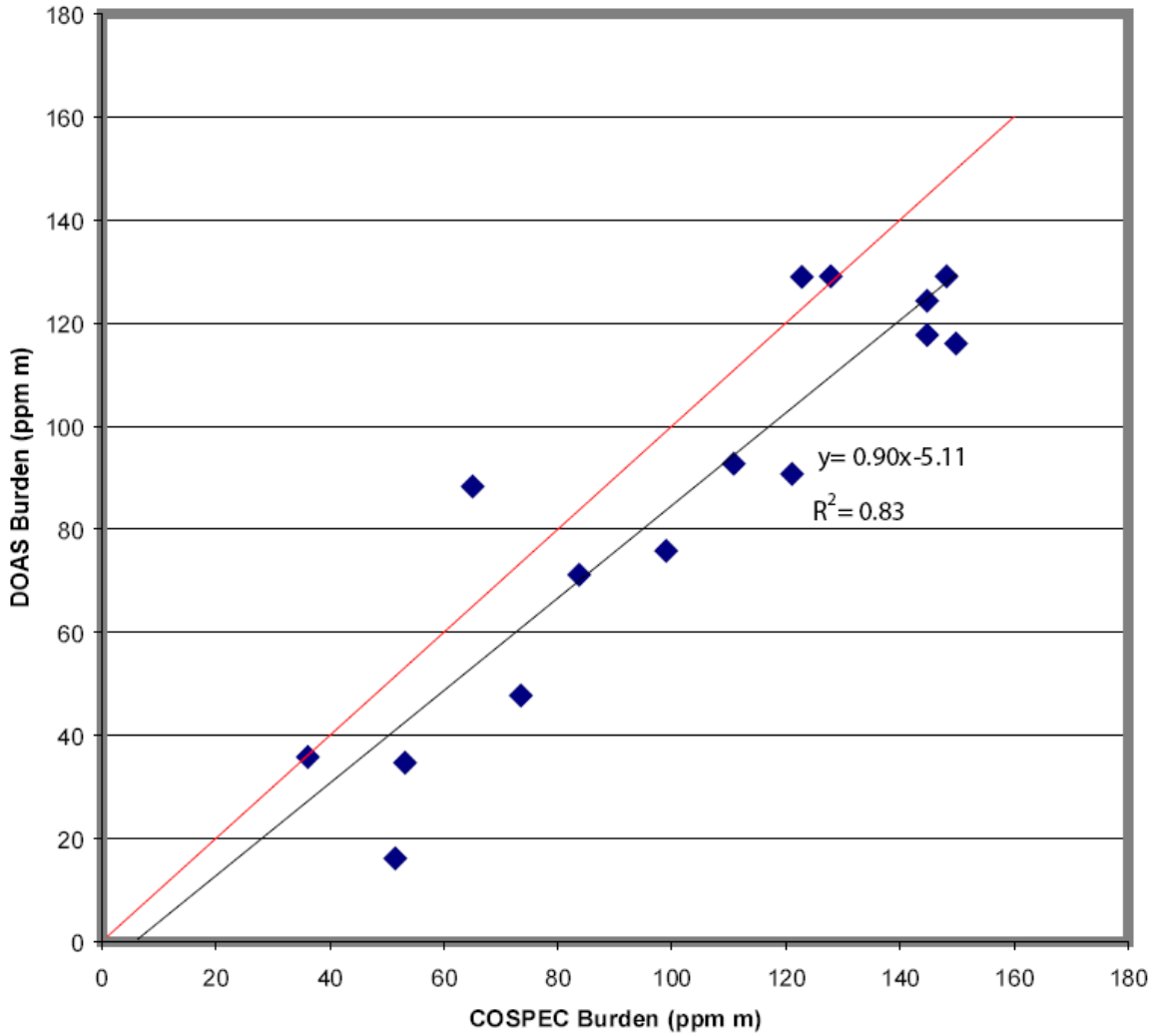

Figure 12: DOAS peak burdens plotted versus COSPEC peak burdens. The R^2 correlation is .83, indicating a good correlation between the two measured burdens. The red line is a one to one line provided for comparison. Note the offset of the line from the origin. This suggests that the DOAS background is approximately 5 ppm m, less than the COSPEC background. This difference is within 1σ.

8. Emission Rates

8.1 COSPEC

SO_2 emission rates were typically determined from data collected over 2-5 days each year between 1992 and 2003 (Table 4) (Fig. 7). Fluctuations in the individual emission rate measurements were observed and exceed the instrument precision. Apparent trends include increasing, decreasing and cyclic emission rates. Generally, the average annual rates increased from 52 ± 16 Mg/day (0.6 kg/s) in 1992 to 85 ± 25 Mg/day (1 kg/s) in 2003 (Table 5). Kyle et al. (1994) suggested SO_2 fluxes decreased significantly in 1984 after debris from large strombolian eruptions buried the lava lake. Since 1984, the lava lake area increased and this coincided with increased SO_2 emission rates between 1985 and 1991 (Kyle et al., 1994). Estimates of the lava lake area between 1980 and 2003 are given in Table 2. During the 2004 season, Werner vent evolved into a small lava lake measuring 1000 ± 100 m^2 while the main lava lake area measured 1400 ± 100 m^2 (Calkins, 2006). There is a correlation between SO_2 emission rate and lava lake area (Fig. 13). The correlation is stronger with smaller lava lake areas and emission rates, respectively.

SO_2 emission rates show striking similarity from year to year, indicating a relatively stable magmatic system (Table 5). Despite the fact that SO_2 emissions rate measurements are collected typically in December, I assumed that the observations are generally representative of the annual activity. Moreover, location and measured plume conditions selected for data collection remained the same, providing consistency within the method (Kyle et al., 1997).

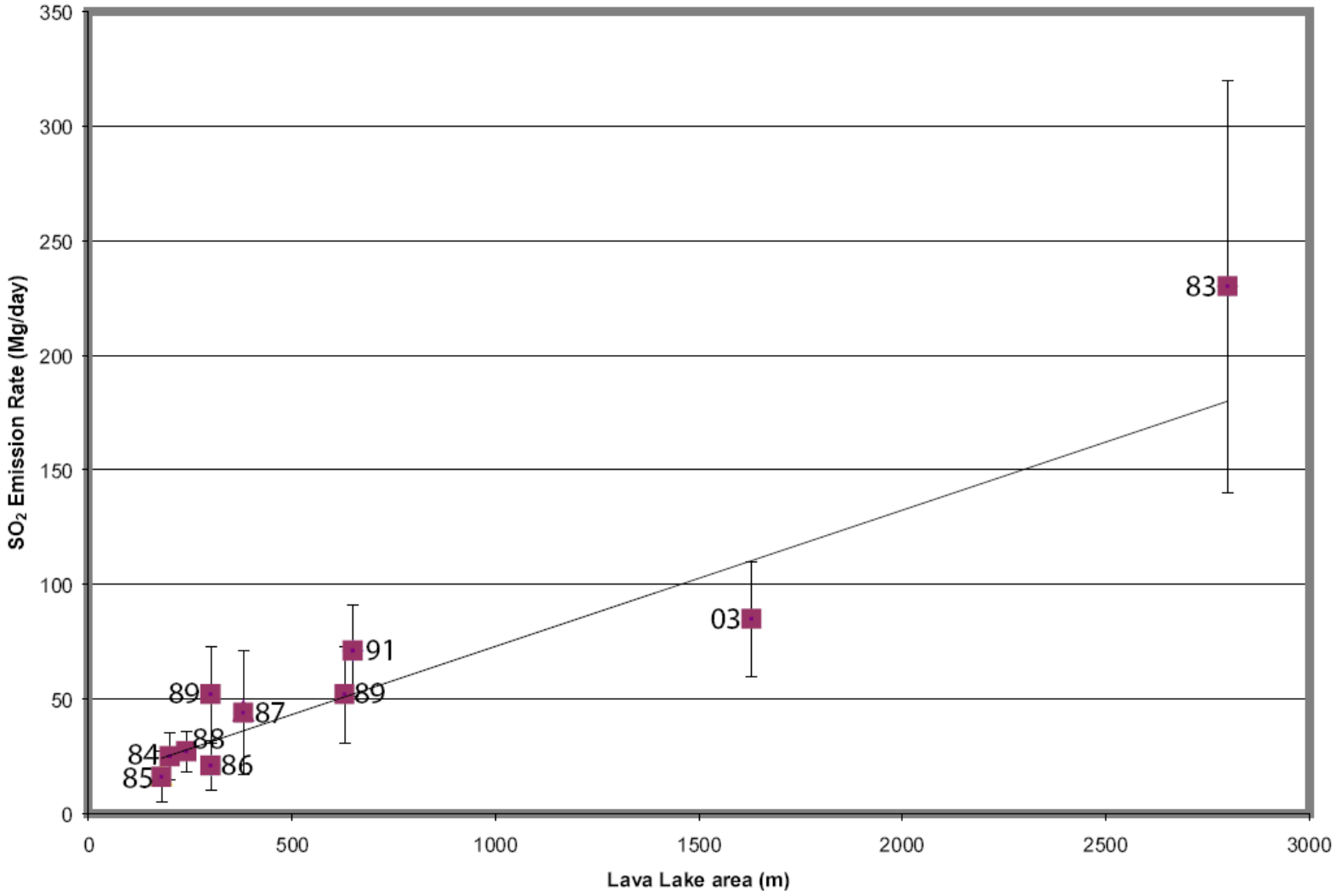

Figure 13: Lava lake area (Table 2) versus SO_2 emission rates (Table 1 and 5). The numbers next to each data point represent the year the data was collected. There is a close correlation between lava lake area and SO_2 emission rate.

8.2 DOAS

DOAS SO_2 emission rate measurements were collected in 2003 and 2005 (Table 6). These are the first DOAS measurements on Erebus volcano. Emission rates vary and show spikes and localized increases and decreases. These variations may represent changes in shallow degassing behavior variations or magma supply into the lava lake (Kyle et al., 1994). Average daily emission rates remained the same, within 1 standard deviation, between 2003 and 2005 (Fig. 14). The small decrease in emission rates between 2003 and 2005 from 95±31 Mg/day to 76±27 Mg/day, can be attributed to a decrease in lava lake area. Systematic trends are difficult to determine with visual inspection and require time series analysis to identify patterns.

9. Eruptions

In 2005 SO_2 emission rates were collected prior to and after two strombolian eruptions (Fig. 15). Emission rates directly before the first eruption were ~50 Mg/day (0.6 kg/s). Assuming a rise rate of 5 m/s, the gas from an eruption will take ~40 seconds to reach the crater rim.

The first eruption occurred at 12:55:09 (local time). The gas from this eruption was measured 38 seconds later at 12:55:47. The emission rates prior to this eruption averaged 57 Mg/day (0.66 kg/s). The measured emission rate for the eruption was 39 Mg/day (0.5 kg/s). This is lower than the emission rates measured before the eruption.

A second eruption occurred at 13:06:13. The gas from this eruption was measured 36 seconds later at 13:06:49. Prior to this eruption, emission rates averaged 67

Table 6: Daily SO_2 emission rates from Erebus volcano obtained with DOAS during the 2003 and 2005 austral summer field season.

Year	Date	N*	Mode	Flux Mg/day (kg/s)
2003	6 Dec	1	Snowmobile	26 (0.3)
	7 Dec	4	Snowmobile	20±5** (0.23±0.06)
	11 Dec	13	Helicopter	74±17 (0.86±0.20)***
	11 Dec	2	Snowmobile	24, 5 (0.28, 0.06)
	11 Dec	41	Stationary scan	95±31 (1.01±0.36)
2005	11 Dec	409	Stationary scan	73±25 (0.84±0.29)
	12 Dec	404	Stationary scan	78±29 (0.90±0.34)

* N- number of measurements
** SD- Standard deviation
*** Oppenheimer et al., 2005

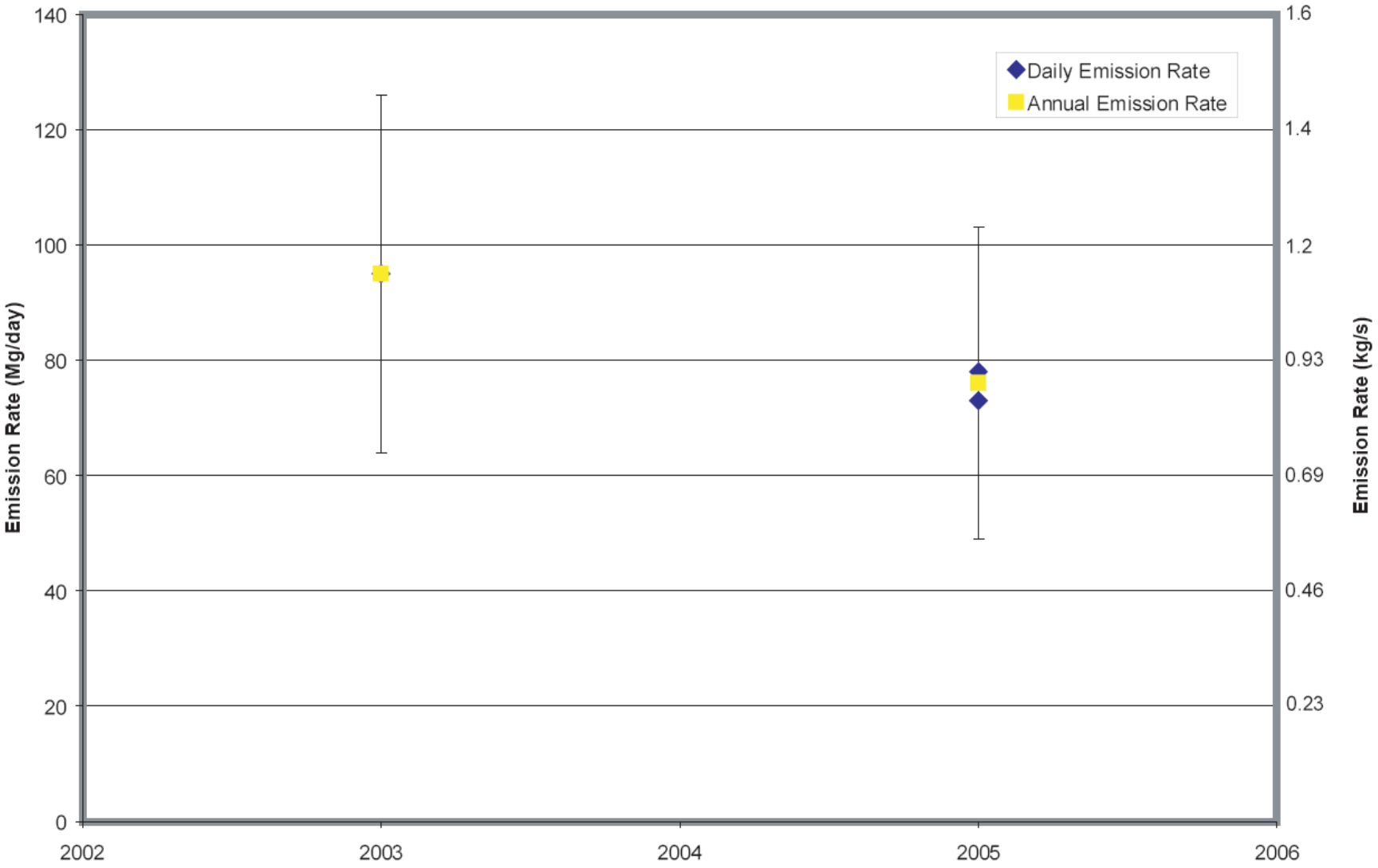

Figure 14: Average daily and average annual emission rates for 2005 and the annual emission rate for 2003 collected with DOAS. Standard deviations are denoted with error bars on the annual emission rates. The slight decrease in emission rate is probably related to the lava lake area decreasing from 2100 m^2 to 1400 m^2.

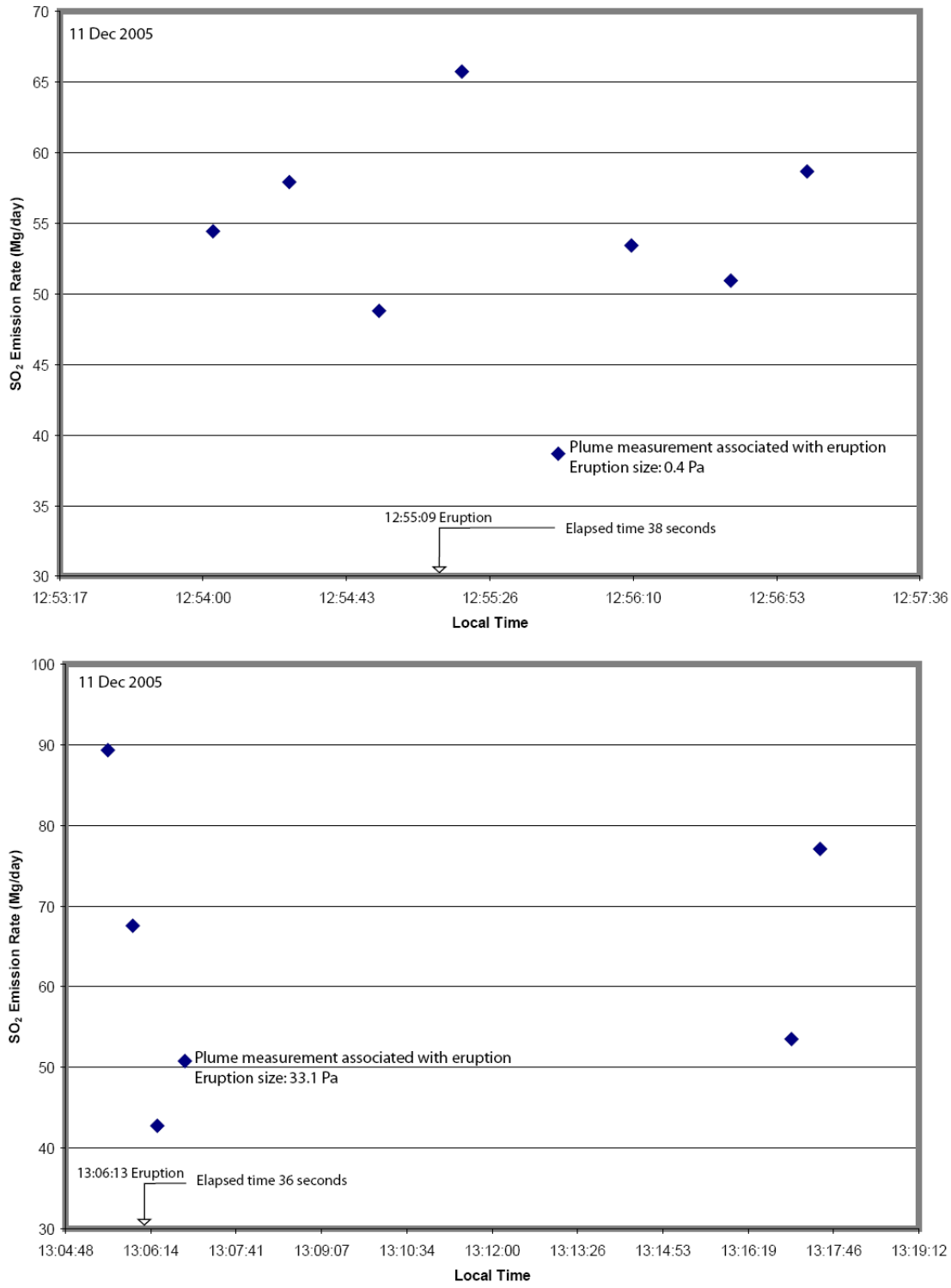

Figure 15: SO_2 emission rates measured by DOAS during small strombolian eruptions in December 2005. Assuming a plume rise rate of 5 m/s and the crater rim is ~200 m above the lava lake, it should take ~40 seconds for the eruption to reach the crater rim and thus be detected with the DOAS. Emission rates preceding and following the eruptions are within 1 standard deviation of the emission rate associated with the eruptions. Note the time scales are different on the two graphs.

Mg/day (0.77 kg/s). The measured emission rate for the second eruption was 51 Mg/day (0.6 kg/s).

These fluctuations are within the range of variations observed during passive degassing. Strombolian eruptions create larger bubbles than those created during passive degassing. If the SO_2 content of the gas were constant the larger bubbles should contain more SO_2 than the smaller bubbles. The SO_2 data suggests that there is no systematic increase associated with eruptions versus passive degassing. Therefore the larger bubbles apparently contain less SO_2, by volume, than the smaller bubbles, which could be consistent with derivation from greater depth. These observations suggest that the eruption gas source is not the same as the passive degassing gas source (Kyle et al., 1994; Oppenheimer, pers. comm.). One plausible explanation for the different compositions is that the gases that drive the strombolian eruptions are derived from deeper seated magmas (Kyle et al., 1994). Fourier Transform Infrared (FTIR) data collected during the eruptions also suggests that there is a separate gas source for the eruptions (Oppenheimer, pers. comm.). Passive degassing apparently continues without being appreciably affected by the ascending eruptive gas slug. Vergniolle and Mangan (2000) state that high bubble ascent rates reduce bubble coalescence. Therefore, primitive gas slugs may not appreciably mix with surrounding gas because they ascend too quickly.

10. SO_2 Emission Rate Time Series Analysis

Systematic variations over tens of minutes to hours in SO_2 emission rates suggest there may be periodicity in the degassing process at Erebus volcano (Kyle et al., 1996).

Such variations may help to interpret vent processes and magma convection. Periodicity in degassing has been observed on Kilauea and Stromboli (Chartier et al., 1988; Ripepe et al., 2002). Gas emission rate variations are likely to be a function of the gas-rich magma supply rate to the degassing zone (Stevenson and Blake, 1998). Klimasauskas (1995) noted a 6-8 day cycle in the elemental filter data collected during the 1992 and 1993 field season and attributed it to magmatic overturn. Anecdotal evidence suggests that high SO_2 emissions rates occur during faster lava lake convection (Kyle et al., 1994). Short term fluctuations (minute cycles) remain constant from day to day whereas longer changes (hourly cycles) vary on a daily basis (Fig. 16). Trends range from simple emission rate increases and decreases to visible emission rate cycles.

Time series analysis using the Fast Fourier Transform (FFT) method transforms data from time space to frequency space. However, FFT analysis requires evenly spaced data. The Lomb-Scargle method "weighs the data on a per point basis instead of on a per time basis" and does not require evenly spaced data (Press et al., 1992).

As the automated scanning data was systematically collected at Erebus volcano, it lends itself to time series analysis. The COSPEC data are evenly spaced within certain time frames, but are not continuous throughout the day. Data gaps exist when the scanner was stopped for calibration measurements. I modeled magma convection with time series analysis, using SO_2 emission rates as the input dataset for the Lomb-Scargle method. Table 7 presents time series analysis results. Figure 17 shows select emission rate power spectra. The Lomb-Scargle method identifies periods with significance intervals of 99.9%, 99%, 95% and 90%. I developed conceptual models based on

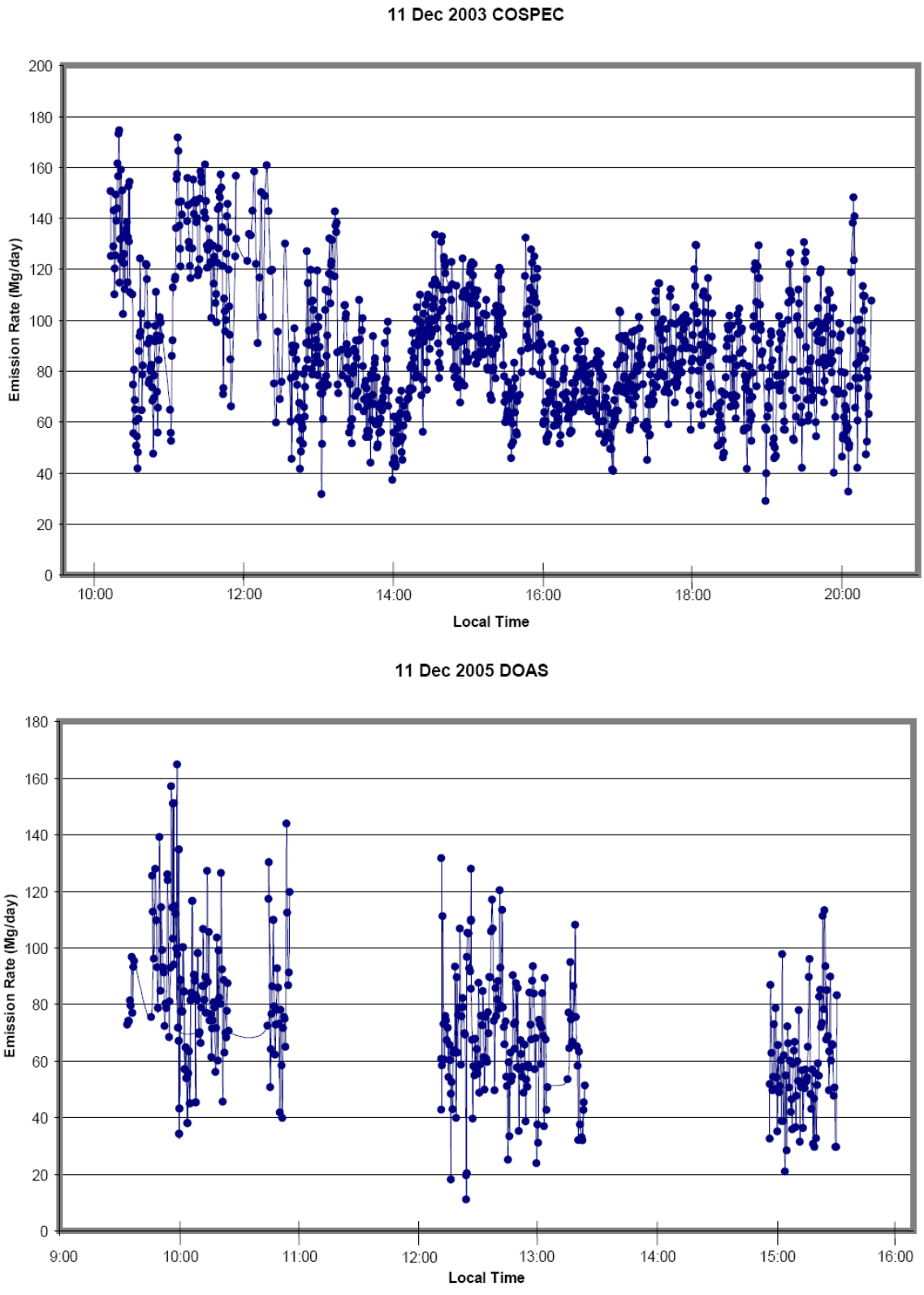

Figure 16: Daily emission rates collected by DOAS and COSPEC showing variability of SO_2 emissions.

Table 7: Time series analysis of SO_2 emission rates using the Lomb-Scargle method.

Spectrometer	Date	Data Set Length (min)	N*	Frequency	Period Min/Cycle	Power	Significance Interval
COSPEC	6-Dec-92	332	146	0.0001134	147	18.4	99.9
				0.0002525	66	24.9	99.9
				0.0004167	40	10.2	90
				0.0009259	18	9.0	90
COSPEC	21-Dec-92	108	114	0.0002688	62	20.4	99.9
COSPEC	7-Dec-93	240	145	0.0001217	137	18.1	99
				0.0004386	38	11.6	99.9
COSPEC	8-Dec-93	173	188	0.0001938	86	12.9	99.9
COSPEC	10-Dec-94	248	65	0.0002193	76	12.6	99.9
				0.000303	55	11.6	99
COSPEC	8-Dec-96	154	73	0.0001082	154	11.1	99
				0.0002165	77	16.7	99.9
				0.0003546	47	11.7	99
COSPEC	10-Dec-96	636	296	4.579E-05	364	11.6	95
				0.0001244	134	34.0	99.9
				0.0001634	102	22.6	99.9
				0.0003876	43	10.1	90
COSPEC	11-Dec-96	345	364	0.0001938	86	16.5	99.9
COSPEC	6-Dec-97	142	144	0.0002058	81	12.4	99
COSPEC	15-Dec-97	365	283	4.566E-05	365	38.0	99.9
				9.158E-05	182	14.2	99.9
				0.0001488	112	15.4	99.9
				0.0002058	81	11.1	95
				0.0002646	63	11.6	95
				0.0003205	52	14.3	99.9

*N is number of measurements

Table 7 cont.

Spectrometer	Date	Data Set Length (min)	N*	Frequency	Period Min/Cycle	Power	Significance Interval
COSPEC	10-Dec-00	449	356	6.485E-05	257	33.8	99.9
				0.0001111	150	25.2	99.9
				0.0001572	106	16.6	99.9
				0.0001938	86	22.6	99.9
				0.0002415	69	12.5	99
COSPEC	12-Dec-00	457	273	6.386E-05	261	58.1	99.9
				0.0001096	152	51.3	99.9
				0.0001543	108	23.5	99.9
COSPEC	6-Dec-03	166	239	0.0003788	44	9.5	90
				0.0012821	13	10.6	90
				0.0015152	11	9.7	90
COSPEC	11-Dec-03	609	1195	6.831E-05	244	48.3	99.9
				0.0001852	90	38.9	99.9
				0.0002604	64	16.2	99.9
				0.000303	55	19.5	99.9
				0.0003968	42	20.3	99.9
				0.000641	26	15.4	99.9
				0.0007246	23	12.3	95
				0.0007937	21	13.8	99
				0.0013889	12	12.7	95
DOAS	11-Dec-05	359	409	8.13E-05	205	16.9	99.9
				0.0001282	130	21.8	99.9
				0.0001852	90	12.8	99.9
				0.0002347	71	13.3	99
				0.0002924	57	14.0	99
				0.0005051	33	10.1	99
DOAS	12-Dec-05	269	404	4.643E-05	359	15.7	99.9
				0.0001389	120	15.1	99.9
				0.0002315	72	18.3	99.9
				0.0003086	54	10.3	99.9
				0.0004167	40	9.8	90
				0.000463	36	17.3	99
				0.0007937	21	10.0	90
				0.0016667	10	15.8	99.9
				0.0016667	10	14.5	99.9

*N is number of measurements

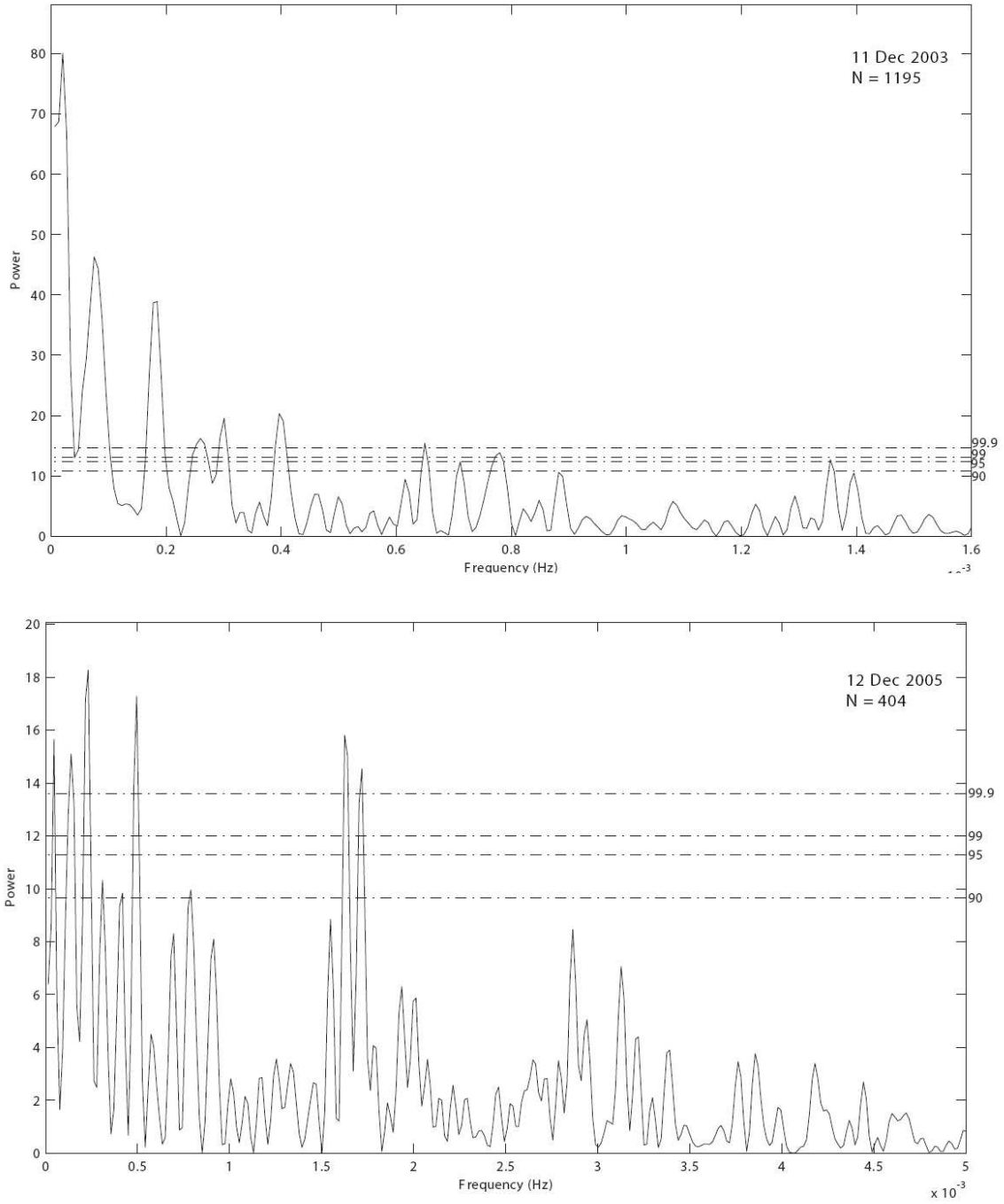

Figure 17: Time series power spectra of SO_2 emission rates produced with the Lomb Scargle method. The dashed lines indicate significance. The top four lines are 99.9%, 99%, 95% and 90% significance. The data within the figures are the significant frequencies that were produced. Higher powers suggest a stronger signal and more significant cycle. The first peak in 11 Dec 2003 yields a frequency longer than the data set duration (600 minutes). This peak was ignored during subsequent analysis.

frequencies with these significance intervals. Output frequencies less than 2 minutes were discarded.

Magmatic processes may not proceed with any precise regularity because of complexities in the physical system. Time series analyses of these processes will not yield sharp peaks but will produce broader peaks. These broad peaks may be a function of the variability in the system. I identified the significant frequencies by listing them in ascending order and looked for clusters of similar period lengths. I considered a frequency significant if the average frequency occurred on at least three different days. COSPEC and DOAS data produced frequencies between 10 minutes and > 300 minutes. The strongest period clusters were identified around 10, 40, 50 and 90 minutes (Fig. 18).

11. SO_2 Degassing Models

Changes in SO_2 emission rates may rise from variations in magma supply rates, physical properties of magma, and atmospheric processes (Stevenson and Blake, 1998). Processes that occur at or near the surface may have a higher frequency of variation in the data than processes that occur at depth, because the bubble do not have to ascend through as much magma. Conversely, if a large obstruction is close to the surface, it may collect bubbles over a long period of time. The bubbles from depth may reach the surface more frequently before the collected bubbles escape the obstruction. However, I suggest that atmospheric and lava lake processes that affect SO_2 flux cycles may account for the shorter cycles yielded from time series analysis. Longer cycles may be attributed to changes occurring deeper in the magmatic system, such as at the lava lake-conduit

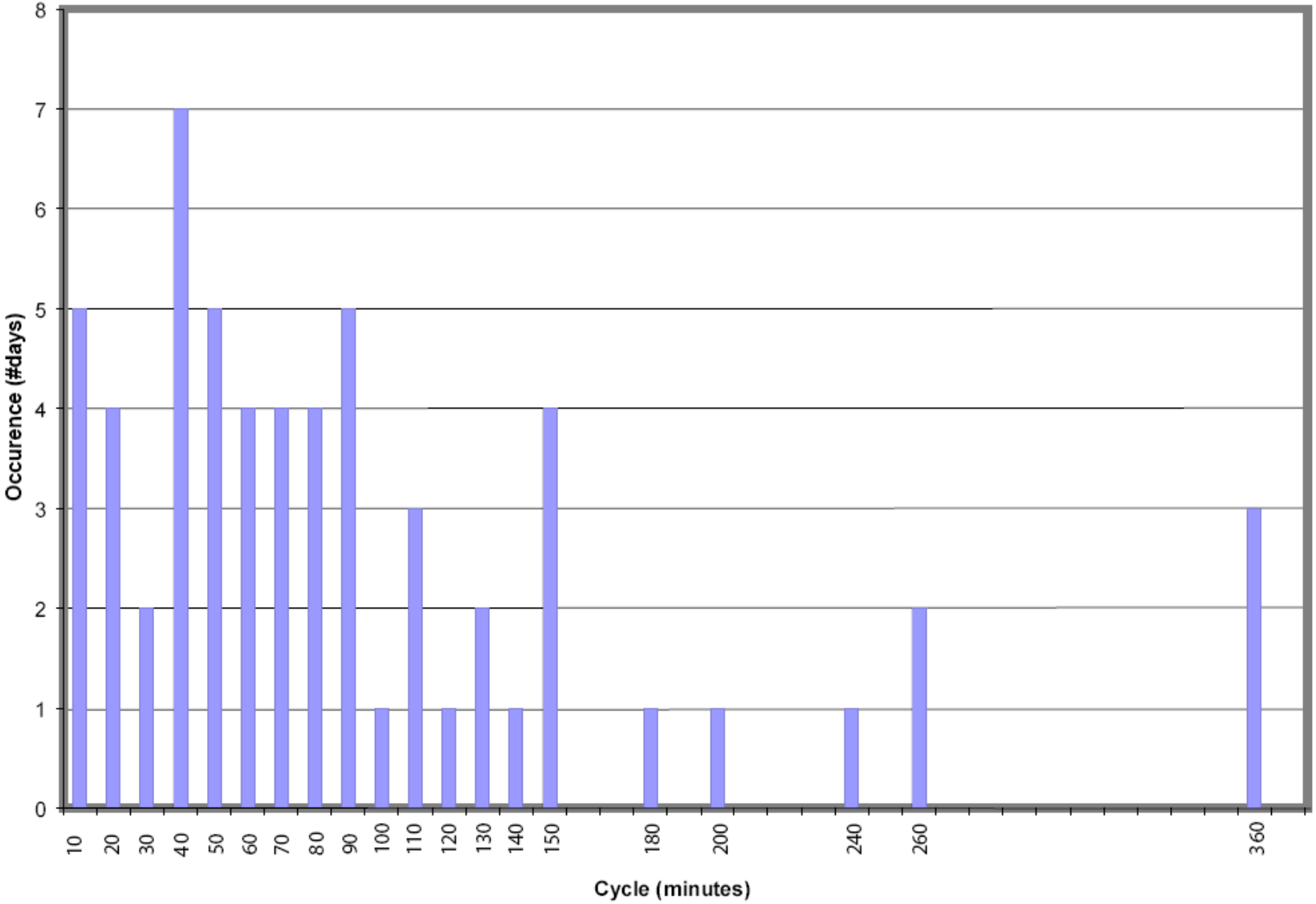

Figure 18: Histogram of all frequencies yielded from time series analysis. Frequencies had to occur on at least three days to be considered significant. Stronger frequencies include 10, 40, 50 and 90 minutes. Weaker frequencies also occur at 20, 60, 70, 80, 110, 150 and 360 minutes.

interface. These changes may be occurring at any of the longer periods listed above (40, 50, 90, 150 and 360 minutes).

11.1 Near Surface Cycles

Several processes can affect SO_2 concentrations in the atmosphere and at the lava lake surface. The main atmospheric process that affects SO_2 fluxes is oxidation from H_2S to SO_2. Kyle et al. (1994) suggests that oxidation of H_2S must occur almost instantaneously as it escapes from the lava lake. So short term cycles are probably best explained with processes that occur within the lava lake.

Puffing is invoked to explain the 10 minute cycle observed in the SO_2 degassing. Puffing is where discrete gas packets, not large enough to be strombolian eruptions, are regularly released from the lava lake surface. Other volcanoes exhibit puffing behavior (Andres et al., 1993; Ripepe et al., 2002) and it has been noted before at Erebus volcano (Kyle et al., 1994). Sharp increases and gradual decreases in the SO_2 signal helped to identify the puffs in the data (Kyle et al., 1994). Moreover, the puffs were visually identified because of their faster rise rates with respect to the rest of the plume. The 10 minute frequency was noted by Kyle et al. (1994) and is supported by FTIR data collected during the 2004 and 2005 seasons (Oppenheimer, pers. comm.). Variable plume circulation within the crater may help explain some of the puffing behavior, but lava lake videos do not show significant variations in plume circulation correlated to puffing. Additionally, the FTIR data, which show the 10 minute cycle, were derived from infrared measurements using the lava lake as a source (Oppenheimer, pers. comm.).

Because the FTIR measures gas near the surface of the lava lake, these FTIR measurements are less likely to be affected by plume circulation within the crater.

If the puffs are rising faster, then they must have a steeper thermal contrast with the ambient air than the rest of the plume. Fast rising gas packets from deeper, warmer magma chamber may account for the faster rise rates seen in the puffs. However, I interpreted above that eruption gas slugs from the storage chamber are rising too fast to significantly affect passive degassing. Instead, physical obstructions within the lava lake geometry may account for faster rise rates. For example, a small shoulder in the side of the lava lake near the surface would allow bubble accumulation/nucleation and, subsequently, heat accumulation. Once the accumulated bubbles escaped the obstruction, the heat would also escape, creating the steeper thermal gradient needed to make the puffs rise faster. Sparks et al. (1994) acknowledged that short term cycles could be related to bubble accumulation/nucleation and growth. Provided that magma movement was constant, this process could occur at regular intervals. I believe the 10 minute period is related to puffing from the lava lake.

11.2 Deep Seated Cycles

A variety of degassing cycles have been noted at Erebus volcano. Minutes to hour-long cycles are described above. Days-long degassing cycles have also been recognized (Klimasauskas, 1996). However, weather often prohibited SO_2 emission rate collection over many consecutive days, so the following discussion is limited to tens of minutes to hours-long time scales.

Longer frequency variations in SO_2 emission rates may relate to varying magma ascent rate and magma transport scenarios. Events like eruptions can occur quickly, but the frequency between events may be long. Cycle length changes may result from changes in magma chamber geometry or physical magma properties such as viscosity (Aster et al., 2003; Larsen and Gardner, 2004). Ripepe et al. (2002) noted variable fluxes on Stromboli, attributing this to variable magma supply affecting bubble concentration and emission rates. Stevenson and Blake (1998) modeled conduit convection showing that ascent-related cooling caused a viscosity increase, which decreased convection, ultimately reducing the gas flux from the gas rich source. Viscosity increases have also been ascribed to variations in degassing efficiency (Stevenson and Blake, 1998; Sparks, 2003).

I developed two conceptual models to explain SO_2 emission rate periodicity. These models are based either on viscosity changes or magma chamber/conduit geometry (Fig. 19). There is no way to be certain which one of these models is more representative because they are end members. Magma chamber variations readily provide an environment to produce variable emission rates. However, changes in physical magma properties or magma chamber geometry are not mutually exclusive. Furthermore, any combination of these two models may represent a more comprehensive view of degassing behavior.

11.2.1 Viscosity Model

The first model suggests that magma ascent rates can be affected by viscosity increases. Viscosity increases may be a result of decreasing magmatic temperature or

Figure 19: Schematics of two degassing models developed from time series analysis data for Erebus volcano.

Model 1: This model suggests that a slight magma viscosity change could cause slowing of magma ascent. Poiseuille convection flow is modelled after Kazahaya et al. (1994) and Stevenson and Blake (1998). a. A buildup of bubble (red circles) and crystals (blue triangles) causes a viscosity change. The large dashed lines indicate the flow boundary. The small dashed linesindicate the straining ascending magma. b. The viscosity differences can be overcome once a critical pressure, is reached. Arrows indicate direction of flow. Boldness of arrows indicates speed of flow

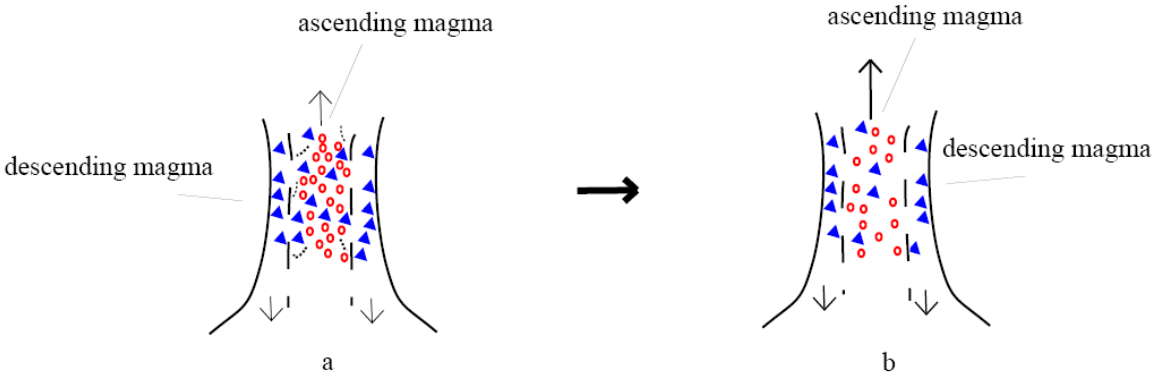

Model 2: Geometric changes in the conduit shape can create gas enclaves where bubbles collect and form a foam, but not enough to form a gas slug. Once the foam reaches a critical size, it escapes to the ascending magma, creating a local increase in gas concentrations that could show up in the flux data Previous workers showed that escaping bubbles must reach a critical value for bubble coalescence to occur (Jaupart and Vergniolle, 1988). The escape of these bubble parcels may happen periodically.

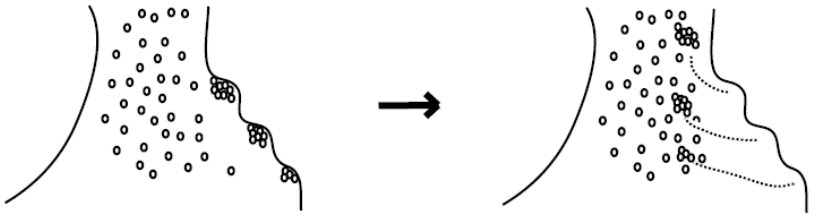

increased bubble or crystal content (Massol and Koyaguchi, 2005). Decompression-related bubble growth occurs as pressure, or depth, decreases, increasing the magma viscosity. Ascent-related cooling may also cause viscosity increases. Fast degassing cycles may represent initial magma degassing before bubble accumulation significantly affects viscosity. As the viscosity increases, the magma convection may decrease. This may manifest as slower degassing cycles in the time series analysis data. As viscosity increases, a critical pressure will be reached, releasing the pressure. After this event, magma transport returns to previous transport rates. Continual interaction between different density and temperature magmas may cause variations in this behavior.

11.2.2 Chamber/Conduit Geometry Model

The second model follows Jaupart and Vergniolle (1988) who modeled Strombolian eruptions as bubbles that collect under an obstruction. Bubbles coalesce and rise to the surface as a slug when a critical pressure or volume is reached. Assuming no viscosity changes occur, my model predicts similar behavior in the Erebus volcano magmatic system. Bubbles collect into a foam which partially collapses allowing intermediate-sized gas pockets to form (Vergniolle and Mangan, 2000). Various cycles may represent different bubble collection areas in the conduit. Increasing magma rise rates also affect bubble coalescence by preventing bubble collision (Vergniolle and Mangan, 2000; Namiki et al., 2003). This allows different sized bubbles to ascend without interacting, which may explain different periods in a sequence of measurements.

12. Magma System Evolution

12.1 Degassed Magma Volume

We can apply the SO_2 flux measurement to determine the minimum magma volume necessary to emit a known amount of gas per unit time (Rose et al., 1982). This is useful in assessing magma chamber volume, magma source constraints and volatile transfer from the earth's interior (Allard, 1997). In addition to the flux measurement, the initial sulfur content is derived from the pre-eruptive sulfur content measured from melt inclusions.

There are several assumptions associated with this model. First, there is no influx of magma. Second, crystallization is negligible and does not affect magma chamber volume. Finally, degassing is assumed to be constant throughout the entire time period.

Typically, the most evolved melt inclusions are used to assess magmatic pre-eruptive sulfur content. Dunbar et al. (1994) showed anorthoclase-hosted melt inclusions formed from partially degassed magmas and work presented in Appendix B showed that olivine-hosted melt inclusions also formed from partially degassed magmas. The partially degassed nature of the melt inclusions suggest they were trapped near the lava lake surface. Hence, the phonolite melt inclusion volatile content is not representative of the initial magmatic volatile concentration. Kyle et al. (1992) consider a tephriphonolite composition for degassing magma even though the lava lake is currently phonolite. Since the phonolite melt inclusions do not represent initial melt concentrations, I used tephriphonolite melt inclusions to estimate the initial sulfur

content. The melt inclusion sulfur content study and all data is discussed in more detail in Appendix C.

A gas plume has been observed at Erebus volcano since at 1963 and probably as early as 1847, emitting SO_2 into the Antarctic atmosphere (Kyle et al., 1982). Between 1963 and 1983, the emission rate is assumed to be 230 Mg/day SO_2 (115 Mg/day S) based on Rose et al. (1985) and visual observations of the lava lake. Annual emission rates from 1984 to the present were averaged and yielded 47 Mg/day SO_2 (23 Mg/day S). Since 1963, Erebus volcano emitted 1.9×10^6 Mg SO_2 (1.9 Mt) into the Antarctic atmosphere. Table 8 displays the model used to determine total magma degassed over 43 years of activity. From 1963 to the present, degassed magma totals 0.61 km^3.

Some of the listed assumptions do not fit the Erebus magmatic system. In Erebus volcano magmas, the crystal content is ~30%, contributing a significant component to Erebus volcano magmas. However, Dunbar et al. (1994) shows that crystallization is not likely to have occurred within the past thirty years. Second, sufficient heat flux must be provided to maintain lava lake activity, requiring either magma influx or a large magma chamber to provide the heat (Dunbar et al., 1994; Harris et al., 1999). There is not data concerning the actual size of the magma chamber at Erebus volcano. So it could be assumed that there is an infinite supply of magma. Finally, degassing has not been constant throughout the 43 years in this model. Degassing rates were significantly higher in the first 20 years of the model than the second half of the model. Despite the discrepancies in the model assumptions, the number presented here is a useful first approximation.

Table 8: Magma volume calculation for Erebus volcano for years between 1963 and present. Degassing was higher between 1963 and 1983 (Rose et al., 1985) so the magma volume was calculated for two periods 1963-1983 and 1984-present. Melt inclusion data found in Appendix C.

S Degassing Rate	Duration	Phonolite Density	Initial S content	End S content	% S lost from magma
230 Mg/day SO_2 115 Mg/day S	1963-1983	2.65 g/cm^3	900 ppm	300 ppm	1-(300/900)= 67%
30 Mg/day SO_2 15 Mg/day S	1984-2006				

1963-1983

115 Mg/day*365.25*10^6= 4.2 x 10^{10} g S degassed per year

4.2x10^{10}/.67=6.3x10^{10} g S degassed from a given magma volume

6.3x10^{10} * (900/10^6) = 7.0x10^{13} g magma to account for sulfur loss

7.0x10^{13} /2.65 = 2.6x10^{13} cm^3= 0.026 km^3 magma degassed in one year

0.026 * 20= 0.53 km^3 degassed in 20 years

1984-2006

15 Mg/day *365.25*10^6 = 5.5 x10^9 g S degassed per year

5.5x10^9/.67= 8.2x10^9 g S degassed from a given magma volume

8.2 x 10^9 * (900/10^6) = 9.1 x 10^{12} g magma to account for sulfur loss

9.1 x 10^{12} / 2.65 = 3.4 x 10^{12} cm^3 = 0.003 km^3 magma degassed in one year

0.003 km^3 * 22 years = 0.08 km^3 magma degassed in 23 years

Total Degassed Magma Volume

0.53 km^3 + 0.08 km^3 = 0.61 km^3 magma degassed in 43 years

12.2 Magma Source and Storage

The small amount of erupted material in a given eruption at Erebus volcano does not account for the large amount of SO_2 degassed. Previous workers called this phenomenon excess sulfur, which has been observed at arc volcanoes including Mt. Pinatubo and Lonquimay and other volcanoes including Mt. Etna and Stromboli (Andres et al., 1991; Wallace and Gerlach, 1994; Wallace, 2001). Geochemical models that incorporate magma mixing (sulfur rich basalt mixing with sulfur poor rhyolite), exsolved gas phases (at top of magma chamber), sulfur-bearing fluids and anhydrite dissolution have been invoked to explain excess sulfur (Andres et al., 1991; Wallace, 2001). Physical processes including magma convection and endogenous growth of the volcanic edifice (internal growth) have also been invoked to explain excess sulfur (Kazahaya et al., 1994; Allard. 1997). Previous work on Kilauea, Mt. Etna and Stromboli showed that consistent passive degassing correlates to endogenous growth of the volcanic edifice (Allard, 1997; Allard et al., 1994; Francis et al., 1993). Two mechanisms contribute to endogenous growth (Francis et al., 1993). Dike intrusion, a common feature in extensional tectonic settings, is the first mechanism. The second mechanism for endogenous growth is cumulate formation, aided by convection via cooling and crystallization. Gerke et al (2005) presented data suggesting that the Erebus volcano magmatic system contains cumulates; though the seismic evidence for cumulates, changing seismic velocity through the cumulate, has not been observed (Aster, pers. comm.) Moreover, seismic evidence for brittle fracture has also not been observed. The magmatic system at Erebus volcano does not exhibit magma mixing, a trapped exsolved gas phase (because of the open nature of the system), anhydrite dissolution or a sulfur-

rich fluid phase. Moreover, lava lake convection has been observed annually (Kyle et al., 1994). The excess sulfur observed at Erebus volcano is interpreted as a consequence of magma convection in a large magmatic plumbing system.

12.3 Convection

Convection on Erebus volcano and other volcanoes is almost certainly driven by density and thermal differences between degassed and non-degassed magma. There are several published models which address detailed mechanisms for density driven convection. Fluid dynamic studies performed by Huppert and Hallworth (2005) propose bi-directional flow as the most important magma convection parameter. Kazahaya et al. (1994) suggested two models of convection. The first model introduces Poiseuille flow in a concentric double walled pipe with degassed magma descending along the outer wall and non-degassed magma ascending through the pipe center (Fig. 20). The second model proposes Stoke's flow, where discrete non-degassed magma spheres ascend through descending degassed magma. Laboratory experiments suggest that Poiseuille flow is a more likely convection model, especially for low viscosity fluids (Fig. 21) (Stevenson and Blake, 1998; Huppert and Hallworth, 2005). Lava lake images collected with a forward looking infrared (FLIR) camera show a central upwelling point supporting Poiseuille flow as the main convective mechanism (Fig. 22) (Calkins, 2006).

Poiseuille flow would suggest that the flux measurements would be relatively consistent, whereas, Stoke's flow would show variable flux rates throughout a given time. Cycles of higher and lower SO_2 flux have been noted at Erebus volcano and these cycles may not be consistent. Huppert and Hallworth (2005) suggest that low viscosity

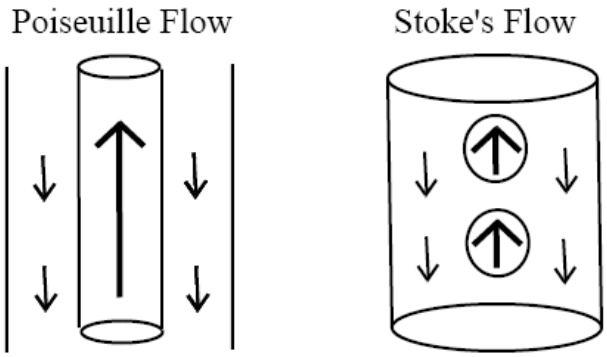

Figure 20: Schematic of a conduit and different models of convection. Poiseuille flow has a single central conduit of rising non-degassed magma whereas Stoke's flow has discrete spheres of non-degassed magma. Flow rate is proportional to size and boldness of arrows. Modified from Kazahaya et al. (1994).

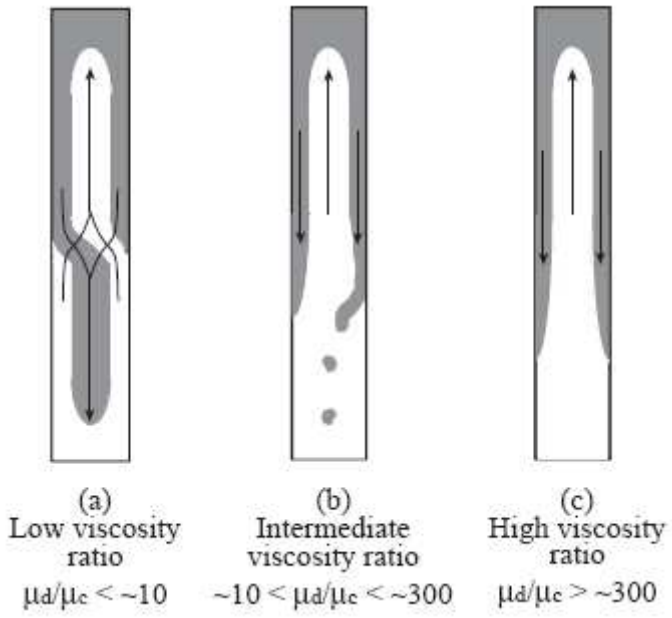

Figure 21: Schematic of conduit flow shows flow changes with viscosity between the non-degassed magma, μ_c, and the degassed magma, μ_d. Modified from Stevenson and Blake (1998).

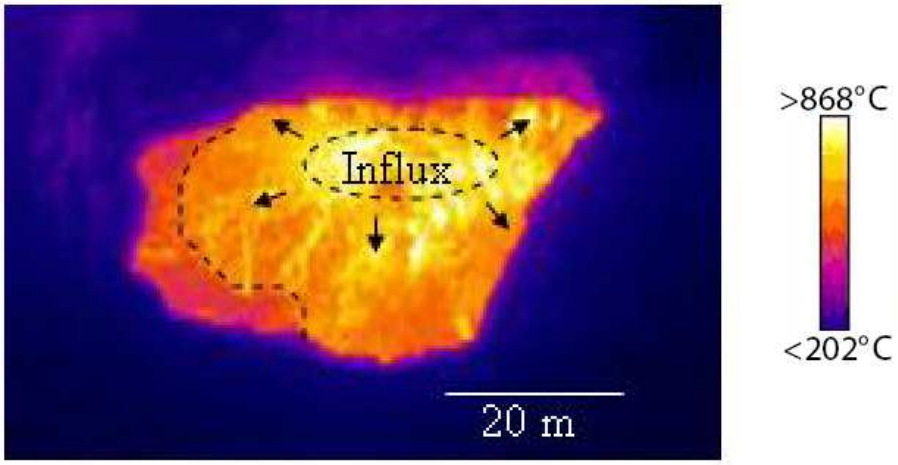

Figure 22: Forward looking infrared (FLIR) image of the main lava lake at Erebus volcano. This image was captured during the 2004 field season. The image shows higher temperature material is upwelling in the center of the lake with downwelling of cooler material around the sides. This suggests hot magma rises in the center and descends along the sides. Modified from Calkins, 2006.

miscible fluids would mix turbulently, which could possibly affect degassing. A combination of Poiseuille and Stoke's flow with turbulent mixing may be a more accurate model of convection at Erebus volcano.

12.4 Sulfur Solubility

SO_2 emission rates relate directly to the amount of sulfur exsolving in a system. Poulson and Ohmoto (1990) linked S solubility with FeO_t content, oxygen fugacity, sulfur fugacity and temperature. Although published sulfur solubility studies do not address anhydrous phonolite magma compositions, there are several anhydrous basalt studies that are applicable to the Erebus volcanic system (Gerlach, 1986; Allard et al., 1994). Kyle et al. (1994) associated Erebus volcano SO_2 emission rates with lava lake area and proposed that S saturation occurs at the lava lake surface. Allard et al. (1994) suggested that exsolution at Stromboli occurs at ≤10 MPa (~300-1000 m) for anhydrous magmas with sulfur contents ≤0.1 wt%. Table 9 provides a geochemical comparison between Stromboli and Erebus volcano. Factors affecting S solubility (FeO and SiO_2) are similar in both systems. Moreover, primitive sulfur contents are similar. Erebus magmas fit the geochemical parameters suggested by Allard et al. (1994) and are geochemically similar to magmas from Stromboli, therefore sulfur exsolution may occur at similar depths (300-1000m).

Table 9: Comparison of primitive and evolved melt inclusion (based on relative SiO_2 content) geochemistry from Mt. Erebus and Stromboli measured with the electron microprobe. Allard et al. (1994) used geochemical parameters to estimate a depth at which sulfur becomes saturated exsolves out of the magma. Stromboli is an anhydrous alkalic basalt and Mt. Erebus is an anhydrous phonolite, but the geochemical controls on sulfur solubility (FeO_t content, SiO_2 content) are similar as are their S concentrations. Therefore is it plausible that sulfur saturation occurs at similar depths on both volcanoes.

Sample name	**Erebus 7713**	**Erebus 97006**	**Stromboli 1990** [α]	**Stromboli 1980**[α]
Mineral host	**olivine (primitive)**	**olivine (evolved)**	**olivine (primitive)**	**diopside (evolved)**
n	**10**	**10**	**3**	**5**
SiO_2	**48.16**	**55.26**	**52.00**	**53.71**
TiO_2	2.76	1.35	1.31	1.26
Al_2O_3	16.92	19.04	16.99	15.67
FeO	**10.83**	**5.74**	**10.11**	**9.30**
MnO	0.27	0.20	16.99	15.67
MgO	2.54	0.88	3.76	4.47
CaO	6.81	2.52	7.33	8.88
Na_2O	6.19	8.41	3.65	2.95
K_2O	3.63	5.74	3.42	2.22
P_2O_5	1.32	0.46	0.84	1.02
S	**0.09**	**0.05**	**0.10**	**0.09**
F	0.29	0.18	NR	NR
Cl	0.10	0.13	0.20	0.16
H_20[β]	0.11	0.08	NR	NR

[α] Allard et al. (1994)
[β] Eschenbacher (1998)
Notes: Geochemical analyses reported in wt% and normalized to 100%. N equals number of analyses. NR equals not reported

13. Atmospheric Effects

13.1 Antarctic Atmosphere

Erebus volcano is a significant source of SO_2 to the Antarctic atmosphere (Zreda-Gostynska et al., 1993). Zreda-Gostynska et al. (1997) estimated Erebus volcano contributed 3% of the total sulfur to the Antarctic atmosphere, using the equation

$$Q = C_{air}\, v_{wind}\, A_c \qquad (3)$$

Where Q is S contribution, C_{air} is SO_4^{2-} concentration in air, A_c is vertical cross-section of air and v_{wind} is wind velocity. They calculated a total atmospheric S (converted to SO_4^{2-}) input of 1300 Gg/year (3559 Mg/day SO_4^{2-}). SO_2 emission rates from Erebus volcano increased from ~70 Mg/day (0.8 kg/s) to ~80 Mg/day (0.9 kg/s) between 1992 and 2003. Therefore, the S contribution to the atmosphere increased from 3% to 4%. Klimasauskas (1995) predicted that Erebus volcano contributes from 10-100% SO_2 to the South Pole troposphere, under ideal conditions. He also noted that effects of increased atmospheric S from Erebus volcano would only be felt at elevations similar to Mt. Erebus (3.7km)

Elevated atmospheric S concentrations can affect atmospheric chemistry processes. First, SO_2 oxidation occurs within days into SO_4^{2-} through the following mechanism (Finalyson-Pitts and Pitts, 2000).

$$OH + SO_2 \rightarrow HOSO_2$$

$$HOSO_2 + O_2 \rightarrow HO_2 + SO_3$$

$$SO_3 + H_2O \rightarrow 2H_2+ + SO_4^{2-}\ (H_2SO_4)$$

Finlayson-Pitts and Pitts (2000) show the SO_2 lifetime, with respect to the only major oxidant OH, is ~13 days. SO_2 in the troposphere also reduces the amount of UV present,

which in turn reduces the amount of O_3 photolyzed to OH, the largest tropospheric oxidizer (Andres and Kasgnoc, 1998). Sulfate particles also act as cloud nuclei which can affect cloud lifetimes (Andres and Kasgnoc, 1998).

13.2 Global Context

Volcanic gases profoundly affect human populations and the climate. The eruption of Mt. Pinatubo in 1991 ejected 20 Mt (Megatons) SO_2 into the stratosphere (Wallace and Gerlach, 1994). Global temperatures decreased for two years because of the elevated sulfate aerosol input (converted from volcanic SO_2) into the stratosphere. This subsequently changed the Earth's albedo, heated the stratosphere, and cooled the trophosphere and Earth's overall temperature (Bluth et al., 1993; McCormick et al., 1995).

The contribution of S from Erebus volcano to the Antarctic S budget is more significant than the global contribution due to the lack of anthropogenic S in the Antarctic atmosphere (Zreda-Gostynska et al., 1993). The average Erebus volcano SO_2 emission rate is ~80 Mg/day (0.9 kg/s), which is low compared to degassing volcanoes elsewhere. Mt. Etna emits the most volcanic SO_2 in the world, ~ 4000 Mg/day (Andres and Kasgnoc, 1998). Andres and Kasgnoc (1998) calculated the annual volcanic SO_2 emission rate of 26,400 Mg/day from continuously degassing volcanoes. Erebus volcano contributes only 0.3% to the global volcanic SO_2 budget, which is ~7 Tg/year and 13% of the anthropogenic SO_2 budget (Andres and Kasgnoc, 1998).

14. Conclusions

Monitoring gas emissions at Erebus volcano for over 20 years provides a large dataset to assess changes in degassing behavior and the magmatic system. The purpose of this study was to determine the sulfur budget and interpret degassing behavior with respect to shallow magma system dynamics. The following conclusions were reached from this work:

(1) SO_2 emission rates from Erebus volcano have been collected from 1992 to 2003 with COSPEC and with DOAS in 2003 and 2005. Individual flux measurements fluctuate greatly throughout a given day. Daily rates are highly variable but they average out to relatively stable yearly rates. There has been an increase in average emission rates since 1996 from 39±17 Mg/day (0.5 kg/s) to ~80±25 Mg/day (0.9 kg/s).

(2) Data collected in 2003 allow comparison between the COSPEC and DOAS methodologies at Erebus volcano. DOAS fluxes are within 10% of COSPEC fluxes when appropriate measures are taken to ensure maximized data collection. The necessary parameters to carefully select or monitor include UV radiation levels, light saturation, coadds and measured spectra integration times. Even though the data sets are within 10%, COSPEC performs more consistently than DOAS due to the high signal to noise ratio in the DOAS data.

(3) Erebus volcano emitted a minimum total of 1.9×10^6 Mg (1.9 Mt) SO_2 into the atmosphere since 1963. The minimum magma volume required to release

this amount of gas is 0.61 km^3 since 1963. These calculations assume limited affects due to crystallization, constant degassing and no magma recharge.

(4) Lava lake observations show that convection is an important process that affects degassing behavior. Magma convection accounts for large amounts of degassed magma and limited erupted material. Work by Stevenson and Blake (1998) and Huppert and Hallworth (2005) suggest that Poiseuille flow is the most plausible convective overturn mechanism. However, a combination of Stoke's and Poiseuille flow may explain observed data more accurately.

(5) SO_2 emission rate time series analysis results show degassing behavior periodicity from Erebus volcano. The shortest cycle, 10 minutes, relates to puffing within the lava lake. This interpretation is supported with FTIR data. Longer cycles can be interpreted with two conceptual models. The fundamental issue behind these models is that changing magma ascent will affect entrained bubbles, ultimately affecting surface degassing behavior. The viscosity model relies on changing magma viscosity to slow magma ascent rates. The chamber/conduit geomtery model suggests variable conduit wall geometry where bubbles become trapped and released without significant bubble coalescence. A combination of all three models could explain observed degassing cycles. Continued flux measurements would supplement the emission rate dataset. In addition to continued flux measurements, correlation with seismicity and experimental modeling, which are beyond the scope of this paper, should be performed.

(6) SO_2 contribution from Erebus volcano to the Antarctic atmosphere increased from 3% to 4% (S as SO_4^{2-}) following an SO_2 emission rate increase from 1992 to 2005. The affects of increased S in the atmosphere are mostly felt at altitudes similar to the summit (3749 m) and at the South Pole. Erebus volcano's sulfur contribution (0.4%) to the global atmosphere remains a fraction of emissions from other volcanoes even with increased SO_2 emissions.

References

Allard, P., 1997. Endogenous magma degassing and storage at Mt. Etna. Geophysical Research Letters, 24: 2219-2222.

Allard, P., Carbonnelle, J., Metrich, N., Loyer, H. and Zettwoog, P., 1994. Suphur output and magma degassing budget of Stromboli volcano. Nature, 368: 326-330.

Anderson, A.T. and Wright, T.L., 1972. Phenocrysts and glass inclusions and their bearing on oxidation and mixing of basaltic magmas, Kilauea Volcano, Hawaii. American Mineralogist, 57: 188-216.

Andres, R.J. and Kasgnoc, A.D., 1998. A time-averaged inventory of subaerial volcanic sulfur emissions. Journal of Geophysical Research, 103(D19): 25, 251-25,261.

Andres, R.J., Kyle, P.R. and Chuan, R.L., 1993. Sulfur dioxide, particle and elemental emissions from Mount Etna, Italy during July 1987. Geologische Rundschau, 82(4): 687-695.

Andres, R.J., Rose, W.I., Kyle, P.R., deSilva, S., Francis, P., Gardeweg, M. and Moreno, H., 1991. Excessive sulfur dioxide emissions from Chilean volcanoes. Journal of Volcanology and Geothermal Research, 46: 323-329.

Aster, R.C., 2006. Personal Communication.

Aster, R.C. et al., 2003. Very long period oscillations of Mount Erebus Volcano. Journal of Geophysical Research, 108(B11): 2522-2543.

Bluth, G.J.S., Schnetzler, C.C., Krueger, A.J. and Walter, L.S., 1993. The contribution of explosive volcanism to global atmospheric sulphur dioxide concentrations. Nature, 366: 327-329.

Calkins, J., 2006. Ground-based thermal observations of two lava lakes at Mount Erebus Volcano, Antarctica in December 2004. Unpublished Indepedent Study Thesis, New Mexico Institute of Mining and Technology, Socorro, NM.

Carroll, M.R. and Rutherford, M.J., 1988. Sulfur speciation in hydrous experimental glasses of varying oxidation state: Results from measured wavelength shifts of sulfur X-rays. American Mineralogist, 73: 845-849.

Carroll, M.R. and Webster, J.D., 1994. Solubilities of sulfur, noble gases, nitrogen, chlorine, and fluorine in magmas. In: M.R. Carroll and J.R. Holloway (Editors), Volatiles in Magmas. Reviews in Mineralogy. Mineralogical Society of America, Washington D.C., pp. 231-280.

Chartier, T.A., Rose, W.I. and Stokes, J.B., 1988. Detailed record of SO_2 emissions from Pu'u O'o between episodes 33 and 34 of teh 1983-1986 eruption, Kilauea, Hawaii. Bulletin of Volcanology, 50: 215-228.

Cooper, A.K., Davey, F.J. and Behrendt, J.C., 1987. Seismic stratigraphy and structure of the Victoria Land Basin, western Ross Sea, Antarctica. In: A.K. Cooper and F.J. Davey (Editors), The Antarctica Continental Margin: Geology and Geophysics of the Western Ross Sea. Circum-Pacific Council for Energy and Mineral Resources, Earth Sciences Series, Houston, TX, pp. 27-76.

Daag, A.S., Tubianosa, B.S., Newhall, C.G., Tuñgol, N.M., Javier, D., Dolan, M.T., Delos Reyes, P.J., Arboleda, R.A., Martinez, M.M.L, and Regalado, M.T.M, 1996. Monitoring sulfur dioxide emission at Mount Pinatubo. In: C. Newhall and R.S. Punongbayan (Editors), Fire and Mud: Eruptions and Lahars of Mount Pinatubo, Philippines. University of Washington Press, Seattle and London.

Danyushevsky, L., McNeill, A. and Sobolev, A., 2002. Experimental and petrological studies of melt inclusions in phenocrysts from mantle-derived magmas: an overview of techniques, advantages and complications. Chemical Geology, 183(1-4): 5-24.

Danyushevsky, L.V., Della-Pasqua, F.N. and Sokolov, S., 2000. Re-equilibration of melt inclusion trapped by magnesian olivine phenocrysts from subduction-related magmas: petrological implications. Contributions to Mineralogy and Petrology, 138: 68-83.

Davies, A. et al., 2005, submitted. Monitoring Active Volcanism with the Autonomous Sciencecraft Experiment (ASE) on EO-1. Remote Sensing of Environment.

Delgado-Granados, H., Gonzalez, L. and Sanchez, N., 2001. Sulfur dioxide emissions from Popocatepetl volcano (Mexico): case study of a high-emission rate, passively degassing erupting volcano. Journal of Volcanology and Geothermal Research, 108(1-4): 107-120.

Delmas, R.J., 1982. Antarctic sulphate budget. Nature, 299: 677-678.

Devine, J.D., Sigurdsson, H. and Davis, A.N., 1984. Estimates of sulfur and chlorine yield to the atmosphere from volcanic eruptions and potential climatic effects. Journal of Geophysical Research, 89: 6309-6325.

Dunbar, N.W., Cashman, K.V. and Dupre, R., 1994. Crystallization processes of anorthoclase phenocrysts in the Mount Erebus magmatic system: Evidence from crystal compostions, crystal size distribution, and volatile contents of melt inclusions. In: P.R. Kyle (Editor), Volcanological and Environmental Studies of Mount Erebus, Antarctica. American Geophysical Union, Washington, D.C., pp. 129-146.

Elias, T. et al., 2006. Comparison of COSPEC and two miniature ultraviolet spectrometer systems for SO_2 measurements using scattered sunlight. Bulletin of Volcanology, 68: 313-322.

Eschenbacher, A., 1998. Open-system degassing of a fractionating, alkaline magma, Mount Erebus, Ross Island, Antarctica. M.S. Thesis Thesis, New Mexico Institute of Mining and Technology, Socorro, NM, 89 pp.

Esser, R.P., Kyle, P.R. and McIntosh, W.C., 2004. Ar^{40}/Ar^{39} dating of the eruptive history of Mount Erebus, Antarctica, volcano evolution. Bulletin of Volcanology, 66(8): 671-686.

Finlayson-Pitts, B.J. and Pitts, J.N., 2000. Chemistry of the Upper and Lower Atmosphere. Academic Press, San Diego, 969 pp.

Francis, P., Oppenheimer, C. and Stevenson, D.S., 1993. Endogenous growth of persistently active volcanoes. Nature, 366: 554-557.

Galle, B. et al., 2002. A miniaturised ultraviolet spectrometer for remote sensing of SO2 fluxes: a new tool for volcano surveillance. Journal of Volcanology and Geothermal Research, 119: 241-254.

Gerke, T.L., Kilinc, A.I. and Sack, R.O., 2005. Ti-content of high-Ca pyroxenes as a petrogenetic indicator: an experimental study of Mafic Alkaline Rocks from the Mt. Erebus volcanic region, Antarctica. Contributions to Mineralogy and Petrology, 148: 735-745.

Gerlach, T.M., 1986. Exsolution of H_2O, CO_2, and S during eruptive episodes at Kilauea Volcano, Hawaii. Journal of Geophysical Research, 91(B12): 2177-2185.

Gerlach, T.M. and Graeber, E.J., 1985. Volatile budget of Kilauea volcano. Nature, 313: 273-277.

Giggenbach, W.F., 1996. Chemical composition of volcanic gases. In: R. Scarpa and R.I. Tilling (Editors), Monitoring and Mitigation of Volcano Hazards. Springer-Verlag, Berlin, pp. 221-256.

Giggenbach, W.F., Kyle, P.R. and Lyons, G., 1973. Present volcanic activity on Mount Erebus, Ross Island, Antarctica. Geology, 1: 135-136.

Glaze, L., Francis, P.W. and Rothery, D.A., 1989. Measuring thermal budgets of active volcanoes by satellite remote-sensing. Nature, 338(6211): 144-146.

Harpel, C., Kyle, P.R., Esser, R.P., McIntosh, W.C. and Caldwell, D.A., 2004. Ar40/Ar39 dating of the eruptive history of Mount Erebus, Antarctica: summit flows, tephra and caldera collapse. Bulletin of Volcanology, 66(8): 687-702.

Harris, A.J.L. et al., 1997. Low-cost volcano surveillance from space: case studies from Etna, Krafla, Cerro Negro, Fogo, Lascar and Erebus. Bulletin of Volcanology, 59(1): 49-64.

Harris, A.J.L., Flynn, L.P., Rothery, D.A., Oppenheimer, C. and Sherman, S.B., 1999. Mass flux measurements at active lava lakes: Implications for magma recycling. Journal of Geophysical Research Solid Earth, 10(104): 7117-7136.

Huppert, H.E. and Hallworth, M.A., 2005. Bi-directional flows in constrained systems. Jounral of Fluid Mechanics, submitted.

Jaupart, C. and Vergniolle, S., 1988. Laboratory models of Hawaiian and Strombolian eruptions. Nature, 331: 58-60.

Klimasauskas, E.P., 1995. Emission and dispersion of gaseous S,F and Cl from Mt. Erebus, Antarctica. Thesis Thesis, N.M. Inst. Mining and Technology, 95 pp.

Kyle, P.R., 1977. Mineralogy and glass chemistry of volcanic ejecta, from Mt. Erebus, Antarctica. New Zealand Journal of Geology and Geophysics, 20(6): 1123-1146.

Kyle, P.R. and Cole, J.W., 1974. Structural control of volcanism in the McMurdo Volcanic Group, Antarctica. Bulletin of Volcanology, 38: 16-25.

Kyle, P.R., Dibble, R.R., Giggenbach, W.F. and Keys, J., 1982. Volcanic activity associated with the anorthoclase phonolite lava lake, Mount Erebus, Antarctica. In: C. Craddock (Editor), Antarctic Geoscience. University of Wisconsin Press, Madison, pp. 735-745.

Kyle, P.R. and McIntosh, W.C., 1989. Automation of a correlation spectrometer for measuring SO_2 emissions, IAVCEI General Assembly.

Kyle, P.R., McIntosh, W.C. and Zreda-Gostynska, G., 1996. Automated correlation spectrometer (COSPEC) measurements of degassing of the anorthoclase phonolite magmatic system, Mount Erebus, Antarctica. New Mexico Institute of Mining and Technology.

Kyle, P.R., Meeker, K. and Finnegan, D., 1990. Emission rates of sulfur dioxide, trace gases and metals from Mount Erebus, Antarctica. Geophysical Research Letters, 17(12): 2125-2128.

Kyle, P.R., Moore, J.A. and Thirlwall, M.F., 1992. Petrologic evolution of anorthoclase phonolite lavas at Mount Erebus, Ross Island, Antarctica. Journal of Petrology, 33(4): 849-875.

Kyle, P.R., Sybeldon, L.M., McIntosh, W.C., Meeker, K. and Symonds, R., 1994. Sulfur dioxide emission rates from Mount Erebus, Antarctica. In: P.R. Kyle (Editor), Volcanological and Environmental Studies of Mount Erebus, Antarctica. American Geoophysical Union, Washington, D.C., pp. 69-82.

Larsen, J.F. and Gardner, J.E., 2004. Experimental study of water degassing from phonolite melts: implications for volatile oversaturation during magmatic ascent. Journal of Volcanology and Geothermal Research, 134: 109-124.

Massol, H. and Koyaguchi, T., 2005. The effect of magma flow on nucleation of gas bubbles in a volcanic conduit. Journal of Volcanology and Geothermal Research, 143: 69-88.

McCormick, M.P., Thomason, L.W. and Trepte, C.R., 1995. Atmospheric effects of the Mt. Pinatubo eruption. Nature, 373: 399-404.

McGonigle, A.J.S., Inguaggiato, S., Aiuppa, A., Hayes, A.R. and Oppenheimer, C., 2005. Accurate measurement of volcanic SO_2 flux: Determination of plume transport speed and integrated SO_2 concentration with a single device. Geochemistry Geophysics Geosystems, 6(1).

McGonigle, A.J.S. and Oppenheimer, C., 2003. Optical sensing of volcanic gas and aerosol emissions. In: C. Oppenheimer, Pyle D.M., and Barclay J. (Editor), Volcanic Degassing. Geological Society, London, pp. 149-168.

Metrich, N., Berry, A., O'Neill, H. and Susini, J., 2005. A XANES study of sulfur speciation in synthetic glasses and melt inclusions, Goldschmidt Conference. *In Situ* Microanalysis of Trace Elements, Idaho.

Mikelich, S., 2006. Sulfur, Chlorine, Fluorine and Aerosol Emissions from Mt. Erebus, Antarctica: December 2003 and December 2004. Unpublished Indepedent Study Thesis, New Mexico Institute of Mining and Technology, Socorro, NM.

Moffat, A.J. and Millan, M.M., 1971. The application of optical correlation techniques to the remote sensing of SO2 plumes using skylight. Atmospheric Environment, 5: 677-690.

Namiki, A., Hatakeyama, T., Toramaru, A., Kurita, K. and Sumita, I., 2003. Bubble size distributions in a convecting layer. Geophysical Research Letters, 30(15): 1784-1787.

Oppenheimer, C., 2006. Personal Communication.

Oppenheimer, C. et al., 2005. Mt. Erebus, the largest point source of NO_2 in Antarctica. Atmospheric Environment, 39(32): 6000-6006.

Oppenheimer, C., McGonigle, A.J.S., Allard, P., Wooster, M.J. and Tsanev, V., 2004. Sulfur, heat, and magma budget of Erta 'Ale lava lake, Ethiopia. Geology, 32(6): 509-512.

Platt, U., 1994. Differential optical absorption spectroscopy (DOAS). In: M.W. Sigrist (Editor), Air Monitoring by Spectroscopic Techniques. Chemical Analysis Series. Wiley, New York, pp. 27-84.

Poulson, S.R. and Ohmoto, H., 1990. An evaluation of the solubility of sulfide sulfur in silicate melts from experimental data and natural samples. Chemical Geology, 85: 57-75.

Press, W.H., Flannery, B.P., Teukolsky, S.A. and Vetterling, W.T., 1992. Spectral Analysis of Unevenly Sampled Data, Numerical Recipes in FORTRAN77: The Art of Scientific Computing. Cambridge University Press, Cambridge, pp. 569-577.

Ripepe, M., Harris, A.J.L. and Carniel, R., 2002. Thermal, seismic and infrasonic evidences of variable degassing rates at Stromboli volcano. Journal of Volcanology and Geothermal Research, 118: 285-297.

Roedder, E., 1984. Fluid Inclusions. Reviews in Mineralogy, 12. Mineralogical Society of America, 644 pp.

Rose, W.I., Chuan, R.L. and Kyle, P.R., 1985. Rate of sulphur dioxide emission from Erebus volcano, Antarctica, December 1983. Nature, 316(6030): 710-712.

Rose, W.I., Stoiber, R.E. and Malinconico, L.L., 1982. Eruptive gas compositions and fluxes of explosive volcanoes: budget of S and Cl emitted from Fuego volcano, Guatemala, Andesites. Wiley, New York, pp. 669-676.

Rothery, D.A. and Francis, P., 1990. Short wavelength infrared images for volcano monitoring. International Journal of Remote Sensing, 11(10): 1665-1667.

Rowe, C.A., Aster, R.C., Kyle, P.R., Dibble, R.R. and Schlue, J.W., 2000. Seismic and acoustic observations at Mount Erebus Volcano, Ross Island, Antarctica, 1994-1998. Journal of Volcanology and Geothermal Research, 101: 105-128.

Seaman, S.J., Darby Dyar, M., Marinkovic, N. and Dunbar, N.W., 2006. An FTIR study of hydrogen in anorthoclase and associated melt inclusions. American Mineralogist, 91: 12-20.

Sparks, R., 2003. Dynamics of magma degassing. In: C. Oppenheimer, D.M. Pyle and J. Barclay (Editors), Volcanic Degassing. Geologic Society of London, London, pp. 5-22.

Sparks, R.S.J., Barclay, J., Jaupart, C., Mader, H.C. and Phillips, J.C., 1994. Physical aspects of magmatic degassing I. Experimental and theoretical constraints on vesiculation. In: M.R. Carroll and J.R. Halloway (Editors), Volatiles in Magmas. Reviews in Mineralogy. Mineralogical Society of America, Washington D.C., pp. 413-443.

Stevenson, D.S. and Blake, S., 1998. Modelling the dynamics and thermodynamics of volcanic degassing. Bulletin of Volcanology, 60: 307-317.

Stoiber, R.E., Malinconico, L.L. and Williams, S.N., 1983. Use of the correlation spectrometer at volcanoes. In: H.a.S. Tazieff, J.C. (Editor), Forecasting Volcanic Events. Elsevier, Amsterdam-New York, pp. 425-444.

Symonds, R.B., Rose, W.I., Bluth, G.J.S. and Gerlach, T.M., 1994. Volcanic Gas Studies - Methods, Results, and Applications. In: M.R. Carroll and J.R. Halloway (Editors), Volatiles in Magmas. Reviews in Mineralogy. Mineralogical Society of America, Washington D.C., pp. 1-66.

Symonds, R.B., Rose, W.I., Gerlach, T.M., Briggs, P.H. and Harmon, R.S., 1990. Evaluation of gases, condensate, and SO_2 emissions from Augustine volcano, Alaska: The degassing of a Cl-rich volcanic system. Bulletin of Volcanology, 52: 355-374.

Vandaele, A.C., Simon, P.C., Guilmot, J.M., Carleer, M. and Colin, R., 1994. SO_2 absorption cross section measurements in the UV using a Fourier transform spectrometer. Journal of Geophysical Research, 99: 25599-25605.

Vergniolle, S. and Jaupart, C., 1990. The dynamics of degassing at Kilauea volcano, Hawaii. Journal of Geophysical Research, 95(B3): 2793-2809.

Vergniolle, S. and Mangan, M., 2000. Hawaiian and Strombolian Eruptions. In: H. Sigurdsson (Editor), Encyclopedia of Volcanoes. Academic Press, San Diego, pp. 447-461.

Wallace, P., 2001. Volcanic SO_2 emissions and the abundance and distribution of exsolved gas in magma bodies. Journal of Volcanology and Geothermal Research, 108: 85-106.

Wallace, P.J. and Carmichael, I.S.E., 1994. S speciation in submarine basaltic glasses as determined by measurements of SKα X-ray wavelength shifts. American Mineralogist, 79: 161-167.

Wallace, P.J. and Gerlach, T.M., 1994. Magmatic vapor source for sulfur dioxide relearse during volcanic eruption: Evidence from Mt. Pinatubo. Science, 265: 497-499.

Wardell, L.J., Kyle, P.R. and Chaffin, C., 2004. Carbon dioxide and carbon monoxide emission rates from an alkaline intra-plate volcano: Mt. Erebus, Antarctica. Journal of Volcanology and Geothermal Research, 131: 109-121.

Watson, E.B., 1976. Glass inclusions as samples of early magmatic liquid: Determinative method and application to a South Atlantic basalt. Journal of Volcanology and Geothermal Research, 1: 73-84.

Zreda-Gostynska, G., Kyle, P.R., Finnegan, D. and Prestbo, K.M., 1997. Volcanic gas emissions from Mount Erebus and their impact on the Antarctic environment. Journal of Geophysical Research, 102(B7): 15039-15055.

Zreda-Gostynska, G., Kyle, P.R. and Finnegan, D.L., 1993. Chlorine, fluorine and sulfur emissions from Mount Erebus, Antarctica and estimated contributions to the Antarctic atmosphere. Geophysical Research Letters, 20(18): 1959-1962.

APPENDIX A: METHODS

A.1 Correlation Spectroscopy

Sulfur dioxide (SO_2) emission rates were measured at Erebus volcano using a Barringer correlation spectrometer (COSPEC V) (Stoiber et al., 1983) from 1983 to 2003. COSPEC has been used to measure volcano $_{SO2}$ emissions since the early 1970's (Stoiber et al., 1983), but has, in recent years,b been replaced by the differential optical absorption spectroscopy (DOAS) technique using a miniature ultraviolet spectrometer (Galle et al., 2002). Light enters the COSPEC through a telescope with a 23 by 7 milliradian field of view. After a grating disperses the light, it passes through a spinning correlation disk. Slits etched on the disk filter light at specific wavelengths. These wavelengths, which are between 300 and 315 nm, correlate to positive and negative SO_2 absorption (Stoiber et al., 1983, Millan et al., 1985). A photomultiplier detects the light in the form of volts.

In this study, COSPEC outputs were recorded on a laptop computer equipped with an PCMCIA data acquisition card. In addition to the SO_2 signal, high calibrations, low calibrations, automatic gain control (AGC), and two supplementary signals were logged onto the laptop via three digital inputs and eight analog signals, with an error of ±5 volts.

Calibrations were used in the determination of SO_2 flux, however, the data acquisition program logs the calibrations in volts instead of ppm. The conversion from volts to concentration was obtained when a fused quartz calibration cell of known SO_2 concentration is inserted into the field of view. The voltage is proportional to the concentration recorded and these calibrations were performed every 15-20 minutes.

Ultraviolet light changes intensity throughout the day and can affect the SO_2 flux measurement. One way light affects the measurement is light saturation when the detector reaches its limit of light detection. When this occurs, the flux measurement appears smaller than if the light was not saturated. The changes in light intensity are monitored with the AGC (Fig. 3), which helps to maximize data collection at appropriate times of the day.

Scanning COSPEC measurements were made at the Lower Erebus hut 2100m from the plume as it rose above the crater rim. The COSPEC was mounted on a Pelco model PT1250DC heavy-duty pan/tilt video scanner equipped to automatically scan horizontally but not vertically. Modifications were made to the scanner to allow automatic tilt measurements, which are necessary when the plume is blown horizontally by winds. Stops and associated micro switches on the scanner head were used to adjust tilt and pan (horizontal) angles. Analog signals indicating scan direction and rough scanning rate were obtained from voltage dividers connected to the pan/tilt micro switches. Scan rates are variable from 0.2-2.0° per second with an overall sampling rate of 0.1-1sec. All data (scan rate and angle, etc.) were recorded on the laptop.

The COSPEC data were acquired on the interfaced laptop computer using COSPEC, an in-house data acquisition program written in QuickBasic. After data collection, a user may also assess data quality with the COSPEC program. The program allows data to be examined either graphically or in a tabular form. Following the procedure stated below, a user can obtain a flux measurement with ASPEC, another in-house program written in QuickBasic. Calibrations were identified, reduced and stored using the ASPEC software. Baseline measurements can vary throughout the day and

adjustments are made manually with a mouse click on either side of the calibration to indicate the background SO_2. A typical scan through the plume manifests as a peak in a graphing program. The area under the peak is associated with the SO_2 burden or column abundance, in units of ppm*m. Peak areas were determined by choosing a baseline and the left and right boundaries with the mouse. ASPEC uses this area along with the scan rate, scan angle, the distance to the plume and the plume rise rate to determine the flux (Equation 1).

$$E=0.00023*\cos\theta*B*W_p*RR_p \qquad (1)$$

Where 0.00023 is a conversion factor (Stoiber et al., 1983), $\cos\theta$ is the tilt angle of the COSPEC, B is burden of SO_2 (ppm), W_p is the plume width (m) and RR_p is plume rise rate (m/s). The 0.00023 correction factor takes into account the density of SO_2, an STP factor and the number of seconds per day. Filming the plume and identifiying distinctive characteristics of the plume, such as the leading edge or discoloration, and timing them as they moved through a given distance on the television screen determines the plume rise rate. This distance was calculated using the trigonometry between the known distance of the plume and the Lower Erebus Hut and various topographic landmarks on the crater rim. At times when the plume was not visible the preceding plume rise rate was used.

Most error associated with flux measurements is due to the plume rise rate/wind speed measurement, but there is also operator and instrument noise error (data acquisition cards have ±5 volts) (Stoiber et al., 1983). Filming the plume to obtain plume rise rates reduces the error to ±5%, down from ±40% (Kyle et al., 1994). Operator error has been significantly reduced with the introduction of automated scanning (Kyle et al., 1994).

A.2. Differential Optical Absorption Spectroscopy

Using the differential optical absorption spectroscopy (DOAS) technique, a mini-ultraviolet spectrometer was also used to measure SO_2 emissions during the 2003 and 2004 field seasons. COSPEC data were simultaneously collected in 2003, which allows a direct comparison between the two instruments. Similarly to COSPEC, DOAS uses the absorption of ultraviolet light to measure SO_2 column abundances. This measurement is based on the Beer-Lambert Law (Equation 2).

$$A=\ln(I_o/I)=\sigma NL \qquad (2)$$

Where A is the absorbance of light, I is light intensity in the presence (I) and absence (I_o) of a chemical species, σ is the absorption cross section of a chemical species (cm^2/molecule), N is the concentration (molecules/cm^3) and L is the path length (cm) (Finlayson-Pitts and Pitts, 2000). However, true light intensity cannot be measured because of Rayleigh and Mie scattering (Finlayson-Pitts and Pitts, 1996). Instead a user measures the background light intensity. The Beer-Lambert Law still applies in a modified form (Equation 3)

$$A=\ln(I_o'/I) \qquad (3)$$

Where I_o' is the background light intensity in the absence of a chemical species. As a result, a differential measurement of light intensity is made instead of an absolute measurement. Moreover, DOAS relies on the banded structure of the absorbance cross section of a chemical species with widths of ~5 nm or less to achieve the differential variance needed for the measurement. Platt (1994) provides a review of the technique in further detail.

The difference between COSPEC and DOAS is the order in the data retrieval process at which correlation of the gas occurs (McGonigle and Oppenheimer, 2003). COSPEC correlates instantly with the use of the spinning correlation disc, and this limits the data collected to $_{SO2}$ absorption wavelengths. On the other hand, DOAS collects the entire spectrum from 200 to 400 nm (Galle et al., 2002). Correlation and $_{SO2}$ retrievals are performed when a lab measured spectrum (Vandaele et al., 1994), were scaled to the observed spectrum (McGonigle and Oppenheimer, 2003).

The miniature, ultraviolet spectrometer used at Mount Erebus volcano was similar to that described in Galle et al. (2002). Light is transferred to an Ocean Optics USB2000 spectrometer via a 1-3 m long fiber-optic cable. The cable consists of four 200μm diameter solarization resistant quartz fibers (Galle et al., 2002). The fiber configuration is linear for the spectrometer and circular for the telescopes. The spectrometer uses an asymmetrical Czerny-Turner configuration with a spectral resolution of ~ 0.6 nm over the wavelength range of 200-400nm.

Two types of telescopes were used during the field campaigns on Mt. Erebus. The first telescope is 25 cm long with a 3 cm diameter. It consists of two quartz lenses with a 20 mrad field of view. The second telescope has only one quartz lens and an 8 mrad field of view (Oppenheimer, pers. comm.).

A laptop computer with the custom-built software, DOASIS (http://www.u-phys.uni-heidelberg.de/urmel/doasis/), provides power to the spectrometer as well as a cache for data transfer via a USB cable. DOASIS is also used to retrieve data and run the spectrometer on the variety of data collection platforms, including: helicopter and snow mobile traverses as well as stationary scans. Helicopter and snow mobile traverses used

GPS to ascertain positioning with respect to the plume axis. Location data was collected with HyperTerminal with a 1 second sampling frequency. Wind speed was collected by filming the plume or wind speed measurements taken at the crater rim with a hand-held anemometer.

Listed below is the basic procedure used to obtain a spectrum. Dark spectrum were obtained by preventing light from entering the spectrometer. These were used during data retrieval to exclude spectrometer noise or electronic offset. A background spectrum was collected to ascertain light conditions outside the plume. A number of sample spectra were collected and co-added to yield a single measurement. The number of spectra and sampling interval were changed based on current light conditions to avoid light saturation and to maximize SO_2 detection. For example, in the mid-afternoon, a user could choose 2 co-adds at 500 ms, yielding a single measurement every 1 second. More co-adds would be used in less than ideal light conditions. Typically, measurements were obtained every 1-2 seconds on Mt. Erebus.

Column abundances were obtained through a series of mathematical manipulations of the spectra. First the dark spectrum and background spectrum were subtracted and divided from the observed spectrum, respectively. The spectrum passed through a high-pass filter, after which the log of the spectrum was taken. A low-pass filter was applied to the spectrum. Finally, the spectrum was matched against the high spectral resolution lab spectrum (Vandaele et al., 1994) and run through a non-linear fitting following Platt (1994).

Data reduction was performed using a variety of programs. Data obtained using a mobile platform (helicopter, snow mobile) was reduced using scripts in the DOASIS

software. Stationary scans were reduced using DOASFLUX, a program written in MATLAB and modeled after ASPEC.

APPENDIX B: SO_2 EMISSION RATE TABLES

SO_2 emission rate data was collected annually between 1992 and 2003 with the COSPEC. In 2003 and 2005, data was collected with the DOAS. This section provides all the measured fluxes collected during these field seasons. The data can be found on a CD at the back of this study. The format of the tables includes: time at which the data was collected, scan angle, scan rate, plume width, burden, plume rise rate and SO_2 emission rate in tons/day (equivalent to Mg/day). The average emission rate is also given for each day measurements were collected. COSPEC tables will also include calibration and automatic gain control data.

APPENDIX C: SULFUR OXIDATION STATE AND SULFUR CONTENT STUDY

C.1 Introduction

Melt inclusions, small magma samples trapped in phenocrysts, can provide a petrologic basis for gas geochemistry studies and supply data about the magmatic conditions at cyrstallization. Examples of magmatic conditions include pre-eruptive volatile content, used to determine the total magma degassed by a system (Rose et al., 1985?; Dunbar et al., 1994), and melt redox state (Carroll and Rutherford, 1988; Wallace and Carmicheal, 1992; Danyushevsky et al., (2000)).

In this study, melt inclusions sulfur content was determined for use in conjunction with SO_2 flux data. Melt inclusions were also used to determine the oxidation state of the Mt. Erebus system. Past melt inclusion investigations on Mt. Erebus lavas have developed an anorthoclase and pyroxene crystallization model (Dunbar et al. 1994) and analyzed open-system degassing through fractional crystallization with melt inclusions (Eschenbacher, 1998).

C.2 Methods

C.2.1 Samples

Melt inclusions found in the minerals anorthoclase, pyroxene, olivine and magnetite from Mt Erebus lavas and bombs were investigated for sulfur content and oxidation state (Table C.1). Inclusions in all of the above minerals were used to determine oxidation state, however only olivine-hosted melt inclusions were used in the sulfur content study.

Table C.1: Electron Microprobe samples used in sulfur oxidation state study.

Sample Name	Content	Composition	Location	Reference
7713	Olivine-hosted melt inclusion	Tephri-phonolite	Turks Head	Eschenbacher, 1998
97006	Olivine-hosted melt inclusion	Phonolite	Turks Head	Eschenbacher, 1998
85010	Olivine-hosted melt inclusion, magnetite-hosted melt inclusion	Phonolite	Mt. Erebus Rim	
E96	Olivine-hosted melt inclusion, magnetite-hosted melt inclusion	Phonolite	Mt. Erebus Rim	
dsan82py	Pyroxene-hosted melt inclusion	Phonolite	Mt. Erebus Rim	
dsan82	Anorthoclase-hosted melt inclusion	Phonolite	Mt. Erebus Rim	
dsan04	Anorthoclase-hosted melt inclusion	Phonolite	Mt. Erebus Rim	

C.2.2 Sulfur content

All samples were analyzed using a Cameca SX-100 electron microprobe located at New Mexico Bureau of Geology and Mineral Resources. Samples were examined using backscattered electron (BSE) imagery to identify glass melt inclusions. Quantitative analyses were performed on the melt inclusions and, if present, matrix glass. Elements analyzed include Na, Mg, Al, Si, P, S, Cl, K, Ca, Ti, Mn and Fe. A probe current of 10 nA and an accelerating voltage of 15 kV was used during analyses. Twenty seconds was the typical peak count time for all elements except the following: Na (40s), F (100s), Cl (40s), and S (60s). One half the times for peak count times was used for background counts. Beam size used depended on the melt inclusion size. With the exception of one sample, when 10μm was used, the typical beam size was 25μm.

C.2.3 Sulfur Oxidation State

Sulfur oxidation states were identified using the procedure outlined in Carroll and Rutherford (1988). SKα electrons were emitted from the innermost electron shell when hit with an X-ray beam and their emission wavelength is a signature of the parent element. Oxidation state was determined by the difference in peak position relative to known standards with different valence states. Pyrite and barite were the standards used in this study.

The LPET (d=4.375) was used to scan through a range of sin θ units over 1000 steps. Pyrite and barite were measured before and after each unknown. All wavelength shifts were calculated relative to pyrite, which was used for the S^{-1} boundary. Barite was measured to obtain the S^{+6} boundary and count times were 100 msec for both unknowns

and standards. Operating conditions were: 30-40 nA beam current, 15 kV accelerating voltage, and a 10 μm beam.

C.3 Results

Four samples with melt inclusions were analyzed for sulfur content with ten analyses each. When possible, matrix glass measurements were taken for comparison with melt inclusion sulfur contents. Table C.2 provides the sulfur content results for all samples and certified reference materials. Analytical precision is based on replicate analyses of certified reference materials. Sulfur contents range from 400 ppm (phonolite) to 900 ppm (tephri-phonolite). Matrix glass sulfur contents averaged 400 ppm.

SKα peak centers were determined by fitting a Gaussian curve to the wavelength scan data. The wavelength was calculated using Bragg's law (Equation 1)(Carroll and Rutherford, 1988; Wallace and Carmichael, 1992).

$$n\lambda=2d\sin\theta \qquad (1)$$

Figure C.1 shows the Erebus oxidation state with respect to pyrite and table C.3 shows the same data in tabular format. Calculated oxidation states range from 3.6 (anorthoclase-hosted melt inclusions) to 5.9 (olivine-hosted melt inclusions). Differences in peak position are ± 3 steps, which can translate into a large range in oxidation state. Therefore all the oxidation states listed in table C.3 are within analytical error.

Table C.2: Average Major Element Composition of Olivine-hosted Melt Inclusions and Matrix Glass from Mt. Erebus Volcano, and Average Major Element Compositions of Reference Materials, Determined by Electron Microprobe.[a]

Sample	**7713**		**97006**		**85010 MI**		**Er96 MI**	**85010 Matrix glass**		**Er96 Matrix glass**	
n	**10**		**10**		**2**		**1**	**5**		**4**	
Beam size (μm)	**25**		**25**		**25**		**10**	**25**		**25**	
	MEAN	**SD**	**MEAN**	**SD**	**MEAN**	**SD**		**MEAN**	**SD**	**MEAN**	**SD**
SiO_2	48.16	0.76	55.26	0.34	56.33	0.45	52.74	55.30	0.24	55.08	0.43
TiO_2	2.76	0.17	1.35	0.07	1.13	0.04	1.00	1.07	0.06	1.06	0.04
Al_2O_3	16.92	0.71	19.04	0.17	19.76	0.20	18.04	19.31	0.14	19.45	0.14
FeO	10.83	0.94	5.74	0.12	6.12	0.12	9.14	5.80	0.22	5.77	0.06
MnO	0.27	0.04	0.20	0.03	0.33	0.01	0.54	0.29	0.03	0.31	0.03
MgO	2.54	1.39	0.88	0.03	0.82	0.04	2.94	0.85	0.02	0.85	0.02
CaO	6.81	0.58	2.52	0.20	1.95	0.01	2.20	1.88	0.06	1.94	0.03
Na_2O	6.19	0.59	8.41	0.32	6.89	0.89	7.15	8.99	0.13	8.89	0.11
K_2O	3.63	0.19	5.74	0.11	5.95	0.13	5.06	5.79	0.07	5.78	0.05
P_2O_5	1.32	0.17	0.46	0.10	0.26	0.04	0.78	0.30	0.02	0.29	0.02
F	0.29	0.15	0.18	0.09	0.20	0.28	0.04	0.21	0.06	0.22	0.07
S	0.09	0.02	0.05	0.01	0.04	0.01	0.18	0.03	0.01	0.05	0.04
Cl	0.10	0.01	0.13	0.01	0.17	0.01	0.14	0.14	0.02	0.16	0.01

Sample	**ke12**		**kn18**		**vg2**	
n	**6**		**6**		**4**	
	MEAN	**SD**	**MEAN**	**SD**	**MEAN**	**SD**
SiO_2	69.90	0.46	74.20	0.44	50.80	0.12
TiO_2	0.29	0.03	0.16	0.04	1.88	0.05
Al_2O_3	7.58	0.05	10.53	0.10	14.01	0.10
FeO	8.52	0.08	3.56	0.05	11.84	0.13
MnO	0.26	0.04	0.07	0.03	0.24	0.03
MgO	0.01	0.01	0.00	0.00	6.82	0.05
CaO	0.37	0.01	0.18	0.03	10.93	0.17
Na_2O	7.82	0.43	5.57	0.42	2.69	0.04
K_2O	4.40	0.09	4.69	0.08	0.20	0.02
P_2O_5	0.01	0.01	0.01	0.01	0.23	0.02
F	0.49	0.25	0.70	0.26	0.08	0.04
S	0.03	0.01	0.02	0.01	0.12	0.02
Cl	0.28	0.02	0.31	0.01	0.04	0.02

[a]Notes: Geochemical quantities are in wt.%. Analyses are normalized to 100 wt.%. N equals number of analyses. Analytical precision, based on replicate analyses of standard reference materials of similar composition to the unknown are listed to the right.

	SD
SiO_2	0.45
TiO_2	0.05
Al_2O_3	0.10
FeO	0.08
MnO	0.04
MgO	0.05
CaO	0.17
Na_2O	0.43
K_2O	0.08
P_2O_5	0.02
F	0.25
S	0.01
Cl	0.02

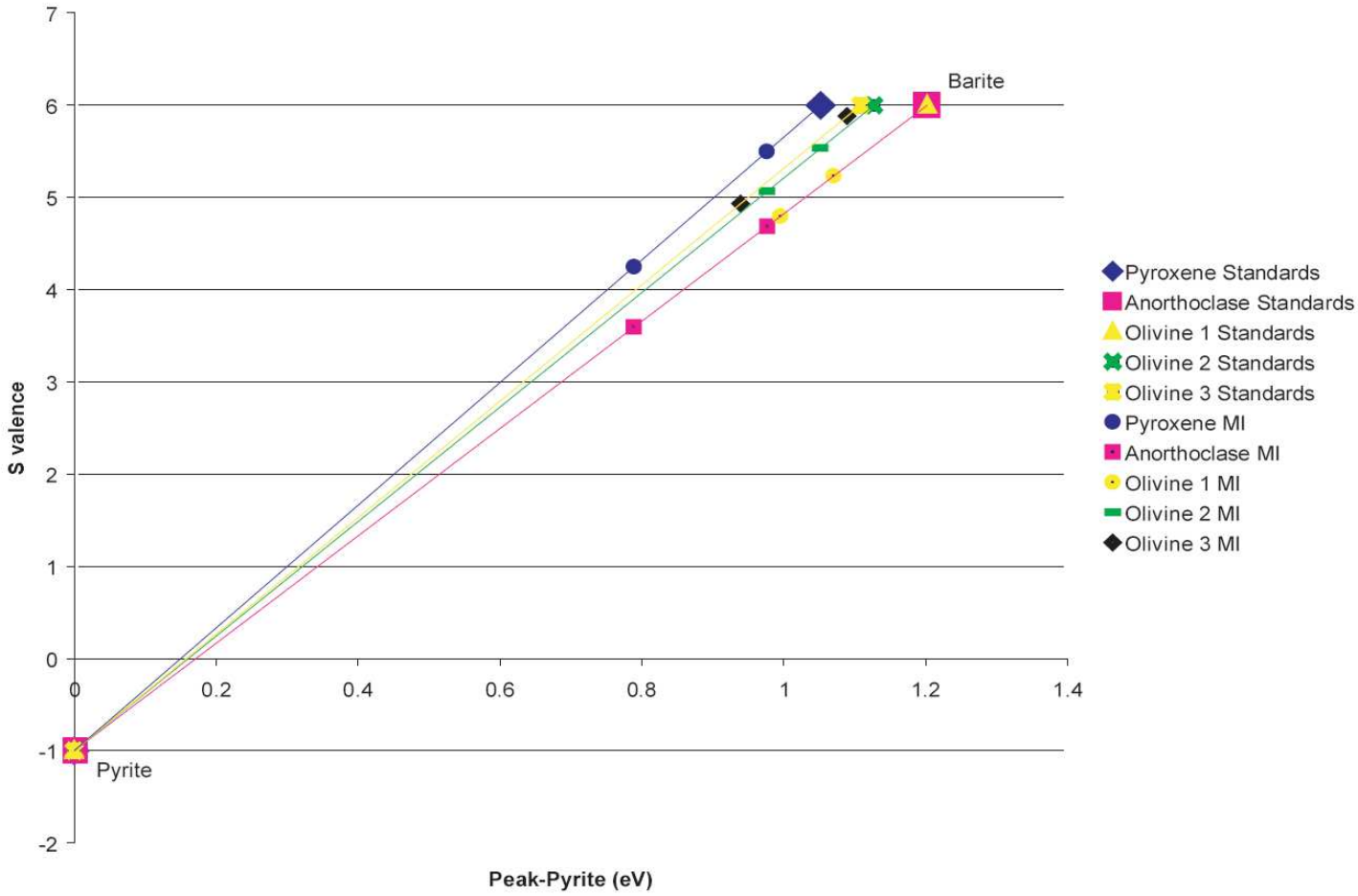

Figure C.1: Sulfur valence state of Mt. Erebus lavas with respect to the pyrite peak position after methods present in Carroll and Rutherford, 1988.

Table C.3: SKα peak positions obtained on the electron microprobe. Valence states were determined relative to pyrite after Carroll and Rutherford (1988).

Mineral	Sample	Peak Position	KeV	Peak Pyrite	S valence
Pyroxene	pyrite 050318	61440	2.3062	0	-1
	dsan82py050318b	61419	2.3070	0.7885	4.249368
	dsan82py050318	61414	2.3072	0.9763	5.499747
	barite 050318	61412	2.3072	1.0515	6
Anorthoclase	pyrite 2	61432	2.3065	0.0000	-1
	dsan0404	61411	2.3073	0.7887	3.592945
	dsan8204	61406	2.3075	0.9766	4.686966
	barite2 050222	61400	2.3077	1.2021	6
Olivine 1	Average Pyrite 1-2	61439.5	2.3062	0.0000	-1
	dsoler96-02 MG	61413	2.3072	0.9951	4.796348
	dsoler96-01 MI	61411	2.3073	1.0703	5.234012
	Average Barite 1-2	61407.5	2.3074	1.2018	6
Olivine 2	Average Pyrite 3-4	61442	2.3061	0.0000	-1
	dsoler96-04 MG	61416	2.3071	0.9763	5.066247
	dsoler96-03 MI	61414	2.3072	1.0514	5.533094
	Average barite 3-4	61412	2.3072	1.1265	6
Olivine 3	Average Pyrite 4-5	61443	2.3061	0.0000	-1
	dsol85-09 MI	61418	2.3070	0.9387	4.931772
	dsol85-10 MG	61414	2.3072	1.0889	5.881304
	Average barite 4-5	61413.5	2.3072	1.1077	6

C.4 Discussion

C.4.1 Sulfur Content

Variations in melt composition may affect sulfur solubility (Carroll and Rutherford, 1994). Decreasing iron content and increasing SiO_2 content allows for decreases in sulfur solubility in a melt (Carroll and Rutherford, 1994). Mt. Erebus lavas follow this trend with sulfur contents decreasing with increasing SiO2. The tephri-phonolite has the highest sulfur content of Mt. Erebus lavas with decreasing sulfur content in the phonolitic samples (Table C.1). Moreover, olivine and anorthoclase – hosted melt inclusions have the same sulfur content. Eschenbacher (1998) also discusses decreasing sulfur content as a sign of continuous degassing throughout fractional crystallization. Sulfur was not retained as an incompatible element is additional evidence for continuous degassing through fractional crystallization.

Mt. Erebus lavas exhibit an unusual characteristic in that both the matrix glass and melt inclusions have the same sulfur content (Dunbar et al., 1994). Previous workers proposed that the magma was slightly degassed when the melt inclusion was enveloped in the host mineral, and suggest a model in which the magma partially degasses at depth causing crystallization to occur (Dunbar et al. (1994). Since olivine is the first silicate mineral to crystallize, we suggest that degassing occurs before olivine cyrstalliztion because the olivine-host melt inclusions and matrix glass have the same sulfur content.

Based on volatile and H_2O content in anorthoclase-hosted melt inclusions, Dunbar et al. (1994) proposed a model in which anorthoclase and pyroxene are crystallized at “near-surface, low pressure” magmatic conditions, possibly after the melt was transported to the surface of the lava lake via convection. Olivine-hosted melt inclusions in this

study show similar characteristics as those in Dunbar et al. (1994), thus we include them in the model discussed in that work.

C.4.2 Oxidation State

Mt. Erebus lavas are considered reduced based on the presence of pyrrhotite as a mineral phase (Kyle, 1978; Kyle et al. , 1992). However, the pyrrhotites are are subhedral, not euhedral, which suggests the melt is oxidizing and the pyrrhotites are resorbing back into the melt. SKα peak positions obtained from olivine, pyroxene and anorthoclase-host melt inclusions also seem to support this hypothesis
Figure C.1 shows that the oxidation state for the melt inclusions ranges from 3.5 to 5.9 with respect to pyrite. Differences in melt inclusion oxidation state were also noted by other workers using X-ray spectroscopy (Métrich et al. (2005)).

Several models have been proposed to explain this behavior (Danyushevsky et al. (2000, 2002); Métrich et al. (2005)). Danyushevsky et al. (2000) proposed re-equilibration occurs when Fe and Mg trade places between the melt inclusion and the host mineral, usually olivine, which they call Fe-loss. A diffusion profile would show a Mg decrease and Fe increased adjacent to the melt inclusion crystal boundary (Fig. C.2). Though a diffusion profile could be obtained on larger melt inclusions, it would be very difficult to obtain a diffusion profile for Mt. Erebus melt inclusion due to their small size (~10 μm). It is unlikely that re-equilibration is occurring in Mt. Erebus melt inclusions for several reasons. First, the melt inclusions studied in Danyushevsky et al. (2000) showed increasing Fe and decreasing Mg in the melt inclusions and vice versa in the host mineral. The Mt. Erebus olivine-hosted melt inclusions do not have significant increases

Figure C.2: Example of diffusion profile collected across a melt inclusion crystal boundary. Note the drop in spike in Fe content and drop in Mg content adjacent to the melt inclusion boundary. After Danyushevsky et al (2000).

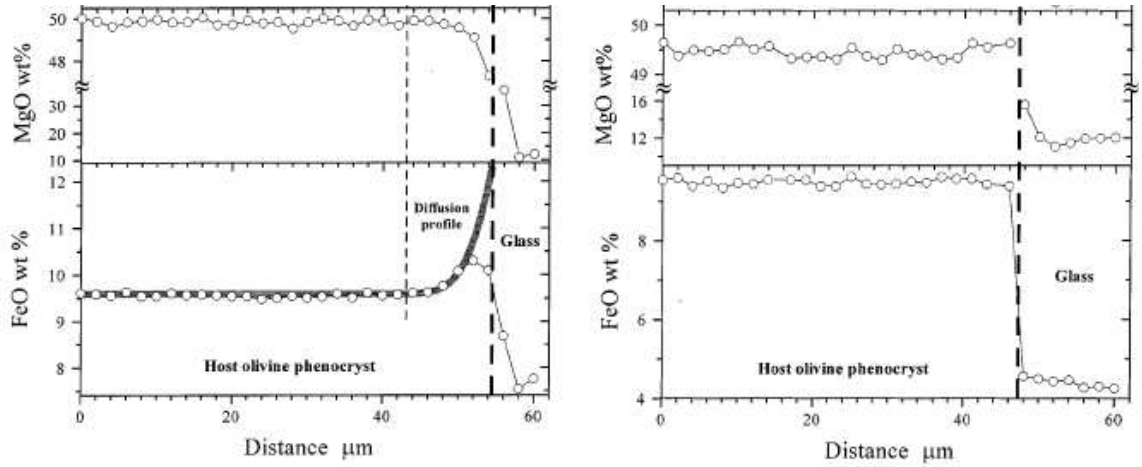

in Mg and decreases in Fe content between different analyses. Second, the olivine-hosted and anorthoclase-hosted melt inclusions have essentially the same Fe and Mg content (Table C.1), suggesting the melt inclusions were derived from the same melt. This also implies the olivines did not form from a more primitive melt.

Another model in Métrich et al. (2005) proposed that melt inclusions may be oxidized post-entrapment on laboratory time-scales. In this case, melt inclusions are trapped at magmatic conditions, which may be reduced. During eruption, the melt inclusion experiences oxidation during flight in a bomb, tephra or ash fall. Since Métrich et al. showed that this was possible in a laboratory time frame, it is entirely possible on eruptive time scales. Finally, the melt inclusions simply could have been entrapped after the magma had been exposed to the air and slightly oxidized, which is possible as shown with the volatile contents.

Several problems must be discussed. Danyushevsky et al. (2000) analyzed melt inclusions ranging from 20 µm to 130 µm, which allowed quantitative diffusion profiles to be collected. Mt. Erebus melt inclusions range from 5 µm to 50 µm. The small size makes it difficult to collect quantitative diffusion profiles. Furthermore, contamination may be a factor from the electron beam hitting the host mineral as well as the melt inclusion.

C.5 Conclusions

Sulfur content was obtained from olivine-hosted melt inclusions using the electron microprobe. Matrix glass and melt inclusions have the same sulfur content which is approximately 400 ppm. Olivine and anorthoclase-hosted melt inclusions have

the same sulfur content. Dunbar et al. (1994) provide a model to explain the melt inclusions and matrix glass having the same sulfur content. Crystals entrapped magma that is partially to fully depleted in volatiles. This implies the crystals are formed at near-surface conditions.

Mt. Erebus lavas are reduced based on the presence of pyrrhotite. Using the SKα peak positions of the melt inclusions, the oxidation state was refined using olivine, pyroxene and anorthoclase-hosted melt inclusions. Mt. Erebus lava redox states range from 3.6 to 5.9. The discrepancy in redox conditions can be explained with two models. Either the melt inclusions were formed under magmatic conditions and oxidized during an eruptive event or they formed from melt that had been slightly oxidized from exposure to air at the lava lake surface.